XGAP's efficient binding with 14-3-3ε and to direct the complex to the ends of the cells, it is possible that the non-GAP domain of XGAP is required for assembling a protein complex that includes PAR proteins; this complex determines the correct positioning of protrusions and accelerates the gastrulation cell movements. On the other hand, we certainly need to further confirm that all these observations obtained with Keller explants indeed represent what is occurring in the deep layer of mesoderm of embryo, which perhaps requires much more sensitive detection systems optimized for *Xenopus* embryo.

The disruption of either xPAR-6 or xPKCλ function causes gastrulation defects (Kusakabe and Nishida, 2004). In addition, 14-3-3ε and aPKC translocate the PAR-1 protein from the inner plasma membrane into the cytoplasm (Kusakabe and Nishida, 2004). PAR proteins, including aPKC, PAR-3, PAR-6, 14-3-3/PAR-5, and PAR-1, are known to comprise an essential system regulating a variety of cellular processes related to cell polarity (Ohno, 2001; Pellettieri and Seydoux, 2002). Therefore, it is reasonable to speculate that a similar, if not identical, system is used to establish the mediolateral polarity of the dorsal mesodermal cells that participate in the gastrulation cell movements in *Xenopus*. It is still unclear, however, how the XGAP and other PAR proteins cooperate to establish cell polarity. One clue may be that PAR-1 expression is often mutually exclusive with that of aPKC/PAR-3/PAR-6 in the cells of several systems. Thus, XGAP and 14-3-3ε may be required to exclude PAR-1 from the plasma membrane, thereby indirectly stabilizing the aPKC/PAR-3/PAR-6 complex near the membrane at the both ends of the cells in the DMZ. To clarify the overall picture of cell polarity establishment in *Xenopus*, a temporal profile of the physical interactions between XGAP and the PAR proteins and the signal regulating XGAP's localization need to be further investigated.

The Possible Role of XGAP in Wnt/PCP Signaling

The noncanonical Wnt/PCP pathway is thought to play a major role in the regulation of gastrulation cell movements. The membrane localization of Xdsh appears to be important for the activation of this pathway (Moriguchi et al., 1999) and for the protrusive morphology in the DMZ or animal cap (Iioka et al., 2004; Wallingford et al., 2000). Therefore, we investigated whether XGAP affects the PCP signaling pathway. However, neither overexpression nor the knockdown of XGAP affected the membrane localization of Xdsh induced by Fz7 in animal caps (data not shown) or changed the induction of the protrusive morphology of the animal cap and DMZ cells ectopically induced by Wnt11 and Fz7 (Figure S3). Given these, we conclude that XGAP is not directly involved in the Wnt/PCP signaling itself.

Recently, we reported that several proteins playing a role in gastrulation; for example, PKC, Arp2/3, actin, and PCP components Xdsh and Rac are localized to the tips of polarized cells undergoing gastrulation (Kinoshita et al., 2003). In addition, a physiological and functional interaction between the PCP pathway and PAR proteins has been reported in *Drosophila* and *Xenopus* (Sun et al., 2001; Ossipova et al., 2005; Djiane et al., 2005). In *Drosophila*, an aPKC/dPatj complex inhibits Fz1-PCP activity without affecting the Fz localization or Dsh recruitment to the membrane (Djiane et al., 2005). Therefore, it is still possible that the confined PAR proteins and PCP signaling in the mediolateral sides are mutually related. It will be interesting to examine in future experiments how the components of PCP and apical-basal polarity cooperate to orchestrate the morphogenetic cell movements by localizing the proteins to the same region of the cells.

Experimental Procedures

Construction of a Keller Explant cDNA Library

About 1000 individual Keller explants were dissected at stage 10.5 and cultured in 0.1% BSA/1× Steinberg's solution. Total RNA was isolated by the acid guanidinium thiocyanate-phenolchloroform method from the explants at stages 11–15, and then 4 μg of poly A+ RNA was oligo-dT primed (XhoI dT primer). A cDNA library was made with the ZAP-cDNA Synthesis Kit (Stratagene) according to the manufacturer's instructions, with minor modifications. After the second-strand synthesis, EcoRI adaptors were ligated and the cDNA was directionally cloned with EcoRI at the 5′ end and XhoI at the 3′ end into the pCS2p+ vector. The average insert size was about 2 kb. The host bacterium was XL2-Blue (Stratagene). The approximately 46,000 individual clones from this library were arrayed by the National Institute for Basic Biology (NIBB), and their ESTs were sequenced by the National Institute of Genetics (NIG), as part of the National BioResource Project in Japan.

Functional Screening

Pools (8–12 clones/pool) of the plasmids were linearized with NotI and used as DNA templates for capped mRNA synthesis by SP6 RNA polymerase with the mMESSAGE mMACHINE kit (Ambion) and purified on a NICK column (Pharmacia). A total of 2 ng of the synthetic mRNA was microinjected into the two dorsal blastomeres of four-cell-stage embryos and screened by observing the morphogenesis after gastrulation. Each clone of the positive pool was then rescreened to isolate a single clone.

Plasmids, mRNA, and Antisense Morpholino Oligonucleotides

Full-length XGAP with or without the 5′UTR, each truncated XGAP, x14-3-3ε, and the xPAR-6 fragments were amplified by PCR and subcloned into a pCS2p+ vector with or without the Venus, RFP, GST, Myc, and Flag tag, respectively. The resXGAP was generated by synonymous substitutions in the Mo targeting region with the following primers: 5′-attgatcaatggcagagccccacaaacaggacatcg-3′ and 5′-cgctcgagttatgatccgtattt-3′.

Plasmids were linearized with NotI. Capped mRNAs were synthesized with the mMESSAGE mMACHINE kit (Ambion) and purified on a NICK column (Pharmacia).

Antisense morpholino oligonucleotides were obtained from GENE TOOLS. The morpholino oligo sequence was constructed over the first Met as follows: XGAP-Mo, 5′-cggttccgccattctccgtctctct-3′. We used the Mo for a scrambled antisense sequence (Ctrl Mo) as a control. Each Mo was injected at 8.3 ng per one blastomere of an embryo.

Embryonic Manipulation

Xenopus eggs were fertilized in vitro as described (Yamamoto et al., 2001), and then capped mRNA or a morpholino oligonucleotide was microinjected into the marginal zone of four-cell-stage embryos. After the injection, the embryos were cultured in 3% Ficol/0.1× Steinberg's solution until the appropriate stage for each experiment.

In Situ Hybridization and RT-PCR Analysis

In situ hybridization was performed with a digoxigenin-labeled RNA probe and alkaline phosphatase substrate (BM purple) (Boehringer Mannheim), as described previously (Harland, 1991). RT-PCR was carried out as reported (Chung et al., 2004). The expression of each mRNA was detected by PCR with the following specific primers: XGAP-F, 5′-aggcacctccccctttaaccgtca-3′; XGAP-R, 5′-acttctctggcaggagggtt-3′; xARG3-F, 5′-gcttctcattcggagcaggtta-3′;

xARG3-R, 5′-acggattctaatgaggcttt-3′. The primer sequences for *Xbra*, *Xwnt11*, *goosecoid*, *myf5*, *otx2*, *chd*, and *ODC*, an internal input control, were as previously described (Chung et al., 2004).

Live-Color Imaging and Time-Lapse Confocal Analysis of Cell Behavior

Live-color imaging in *Xenopus* embryos was carried out as described (Wallingford et al., 2000), with minor modifications. Briefly, 100 pg of the mRNA of a Venus- or RFP-tagged construct was injected into four-cell-stage embryos. Keller explants were isolated from stage 10.5 embryos and cultured in 0.1% BSA/1× Steinberg's solution in a glass-bottomed dish coated with fibronectin (FN) (~0.1 mg/ml, F1141; Sigma-Aldrich) at 13°C for 20–24 hr or at 22°C for 8–12 hr with similar results. The observation was performed just after cells became spindle shaped, when the intercalation started, 5 μm deep in the tissue from the surface of the explant by laser-scanning confocal microscopy with a Carl Zeiss LSM510 microscope.

The protrusive orientation was quantified by counting the active protrusions by time-lapse recording for 10 min at 20°C. The orientation of the protrusion was based on 60° for mediolateral and 120° for anteroposterior sectors, which made the ratio of the orientation in control explants nearly equal to that in a previous report (Wallingford et al., 2000).

Pull-Down Assay Followed by Mass Spectrometry

Pull-down assay followed by mass-spectrometry analysis with the GAP-domain-deleted hARG3 in HEK293T cells was carried out as described (Komatsu et al., 2004), with minor modifications.

Immunoprecipitation

HEK293T cells were transiently transfected with the indicated constructs by the calcium phosphate method. Forty-eight hours after transfection, the cells were lysed in lysis buffer (50 mM Tris-HCl [pH 7.5], 150 mM NaCl, 5 mM EDTA, 0.5% NP-40, 50 mM NaF, 1 mM dithiothreitol, 1 mM sodium orthovanadate, 1 mM [p-amidinophenyl] methanesulphonyl fluoride-HCl, 10 μg/ml aprotinin, 10 μg/ml pepstatin, and 20 μg/ml leupeptin). For coimmunoprecipitation, the lysates were incubated with 10 μl of protein A Sepharose beads and the appropriate antibodies at 4°C overnight. The immunoprecipitates were washed five times with 200 μl of lysis buffer and analyzed by Western blot analysis with the appropriate antibodies. Myc 9E10 (Santa Cruz), Flag M2 (Kodak), antibodies to GFP (MBL), and phospho-serine Q5 (QIAGEN) were used to detect proteins.

Supplemental Data

Supplemental Data including six figures are available at http://www.developmentalcell.com/cgi/content/full/11/1/69/DC1/.

Acknowledgments

We are grateful to Dr. F.M. Watt for the MZ15 antibody; Dr. N. Kinoshita for the mb-Venus and mb-RFP plasmids; Dr. Y. Mimori-Kiyosue for advice on the wound-healing assay; Dr. N. Mizuno for advice on constructing the library; Ms. C. Terasaka, Dr. A. Kitayama, and Ms. H. Nishide for updating the XDB3; Dr. Y. Kohara and Dr. T. Shin-i of the NIG for sequences of the library; and Ms. M. Sugiura for technical assistance. This work was supported by grants from the Japan Society for the Promotion of Science (JSPS), the Ministry of Education, Culture, Sports, Science and Technology (MEXT) (to N.U.), and New Energy and Industrial Technology Development Organization (NEDO) (to T.N.).

Received: August 16, 2005
Revised: February 24, 2006
Accepted: April 17, 2006
Published: July 10, 2006

References

Betschinger, J., and Knoblich, J.A. (2004). Dare to be different: asymmetric cell division in *Drosophila*, *C. elegans* and vertebrates. Curr. Biol. *14*, R674–R685.

Casanova, J.E. (2003). ARFs. Curr. Biol. *13*, R123.

Chung, H.A., Hyodo-Miura, J., Kitayama, A., Terasaka, C., Nagamune, T., and Ueno, N. (2004). Screening of FGF target genes in *Xenopus* by microarray: temporal dissection of the signalling pathway using a chemical inhibitor. Genes Cells *9*, 749–761.

Djiane, A., Yogev, S., and Mlodzik, M. (2005). The apical determinants aPKC and dPatj regulate Frizzled-dependent planar cell polarity in the *Drosophila* eye. Cell *121*, 621–631.

Harland, R.M. (1991). In situ hybridization: an improved whole-mount method for *Xenopus* embryos. Methods Cell Biol. *36*, 685–695.

Heisenberg, C.P., Tada, M., Rauch, G.J., Saude, L., Concha, M.L., Geisler, R., Stemple, D.L., Smith, J.C., and Wilson, S.W. (2000). Silberblick/Wnt11 mediates convergent extension movements during zebrafish gastrulation. Nature *405*, 76–81.

Iioka, H., Ueno, N., and Kinoshita, N. (2004). Essential role of MARCKS in cortical actin dynamics during gastrulation movements. J. Cell Biol. *164*, 169–174.

Keller, R. (2002). Shaping the vertebrate body plan by polarized embryonic cell movements. Science *298*, 1950–1954.

Keller, R., and Danilchik, M. (1988). Regional expression, pattern and timing of convergence and extension during gastrulation of *Xenopus laevis*. Development *103*, 193–209.

Kinoshita, N., Iioka, H., Miyakoshi, A., and Ueno, N. (2003). PKC delta is essential for Dishevelled function in a noncanonical Wnt pathway that regulates *Xenopus* convergent extension movements. Genes Dev. *17*, 1663–1676.

Komatsu, M., Chiba, T., Tatsumi, K., Iemura, S., Tanida, I., Okazaki, N., Ueno, T., Kominami, E., Natsume, T., and Tanaka, K. (2004). A novel protein-conjugating system for Ufm1, a ubiquitin-fold modifier. EMBO J. *23*, 1977–1986.

Kuhl, M. (2002). Non-canonical Wnt signaling in *Xenopus*: regulation of axis formation and gastrulation. Semin. Cell Dev. Biol. *13*, 243–249.

Kusakabe, M., and Nishida, E. (2004). The polarity-inducing kinase Par-1 controls *Xenopus* gastrulation in cooperation with 14-3-3 and aPKC. EMBO J. *23*, 4190–4201.

Liu, X., Zhang, C., Xing, G., Chen, Q., and He, F. (2001). Functional characterization of novel human ARFGAP3. FEBS Lett. *490*, 79–83.

Macara, I.G. (2004). Par proteins: partners in polarization. Curr. Biol. *14*, R160–R162.

Mlodzik, M. (2002). Planar cell polarization: do the same mechanisms regulate *Drosophila* tissue polarity and vertebrate gastrulation? Trends Genet. *18*, 564–571.

Moriguchi, T., Kawachi, K., Kamakura, S., Masuyama, N., Yamanaka, H., Matsumoto, K., Kikuchi, A., and Nishida, E. (1999). Distinct domains of mouse dishevelled are responsible for the c-Jun N-terminal kinase/stress-activated protein kinase activation and the axis formation in vertebrates. J. Biol. Chem. *274*, 30957–30962.

Nagai, T., Ibata, K., Park, E.S., Kubota, M., Mikoshiba, K., and Miyawaki, A. (2002). A variant of yellow fluorescent protein with fast and efficient maturation for cell-biological applications. Nat. Biotechnol. *20*, 87–90.

Nakaya, M., Fukui, A., Izumi, Y., Akimoto, K., Asashima, M., and Ohno, S. (2000). Meiotic maturation induces animal-vegetal asymmetric distribution of aPKC and ASIP/PAR-3 in *Xenopus* oocytes. Development *127*, 5021–5031.

Ninomiya, H., Elinson, R.P., and Winklbauer, R. (2004). Antero-posterior tissue polarity links mesoderm convergent extension to axial patterning. Nature *430*, 364–367.

Nishimura, T., Kato, K., Yamaguchi, T., Fukata, Y., Ohno, S., and Kaibuchi, K. (2004). Role of the PAR-3-KIF3 complex in the establishment of neuronal polarity. Nat. Cell Biol. *6*, 328–334.

Ohkawara, B., Yamamoto, T.S., Tada, M., and Ueno, N. (2003). Role of glypican 4 in the regulation of convergent extension movements during gastrulation in *Xenopus laevis*. Development *130*, 2129–2138.

Ohno, S. (2001). Intercellular junctions and cellular polarity: the PAR-aPKC complex, a conserved core cassette playing fundamental roles in cell polarity. Curr. Opin. Cell Biol. *13*, 641–648.

Ossipova, O., Dhawan, S., Sokol, S., and Green, J.B. (2005). Distinct PAR-1 proteins function in different branches of Wnt signaling during vertebrate development. Dev. Cell *8*, 829–841.

Pellettieri, J., and Seydoux, G. (2002). Anterior-posterior polarity in *C. elegans* and *Drosophila*—PARallels and differences. Science *298*, 1946–1950.

Randazzo, P.A., and Hirsch, D.S. (2004). Arf GAPs: multifunctional proteins that regulate membrane traffic and actin remodelling. Cell. Signal. *16*, 401–413.

Randazzo, P.A., Nie, Z., Miura, K., and Hsu, V.W. (2000). Molecular aspects of the cellular activities of ADP-ribosylation factors. Sci. STKE *2000*, RE1.

Sun, T.Q., Lu, B., Feng, J.J., Reinhard, C., Jan, Y.N., Fantl, W.J., and Williams, L.T. (2001). PAR-1 is a Dishevelled-associated kinase and a positive regulator of Wnt signalling. Nat. Cell Biol. *3*, 628–636.

Suzuki, A., Hirata, M., Kamimura, K., Maniwa, R., Yamanaka, T., Mizuno, K., Kishikawa, M., Hirose, H., Amano, Y., Izumi, N., et al. (2004). aPKC acts upstream of PAR-1b in both the establishment and maintenance of mammalian epithelial polarity. Curr. Biol. *14*, 1425–1435.

Tada, M., and Smith, J.C. (2000). Xwnt11 is a target of *Xenopus* Brachyury: regulation of gastrulation movements via Dishevelled, but not through the canonical Wnt pathway. Development *127*, 2227–2238.

Takeuchi, M., Nakabayashi, J., Sakaguchi, T., Yamamoto, T.S., Takahashi, H., Takeda, H., and Ueno, N. (2003). The prickle-related gene in vertebrates is essential for gastrulation cell movements. Curr. Biol. *13*, 674–679.

Ueno, N., and Greene, N.D. (2003). Planar cell polarity genes and neural tube closure. Birth Defects Res. Part C Embryo Today 69, 318–324.

Wallingford, J.B., Rowning, B.A., Vogeli, K.M., Rothbacher, U., Fraser, S.E., and Harland, R.M. (2000). Dishevelled controls cell polarity during *Xenopus* gastrulation. Nature *405*, 81–85.

Wallingford, J.B., Fraser, S.E., and Harland, R.M. (2002). Convergent extension: the molecular control of polarized cell movement during embryonic development. Dev. Cell *2*, 695–706.

Yamamoto, T.S., Takagi, C., Hyodo, A.C., and Ueno, N. (2001). Suppression of head formation by Xmsx-1 through the inhibition of intracellular nodal signaling. Development *128*, 2769–2779.

Yamanaka, H., Moriguchi, T., Masuyama, N., Kusakabe, M., Hanafusa, H., Takada, R., Takada, S., and Nishida, E. (2002). JNK functions in the non-canonical Wnt pathway to regulate convergent extension movements in vertebrates. EMBO Rep. *3*, 69–75.

Accession Numbers

XGAP (AB195293), *xARF1* (AB195294), *xARF4* (AB195295), and *xARF6* (AB195296) are deposited in GenBank.

The EMBO Journal (2006) 25, 4524–4536 | © 2006 European Molecular Biology Organization | All Rights Reserved 0261-4189/06
www.embojournal.org

THE EMBO JOURNAL

A novel proteasome interacting protein recruits the deubiquitinating enzyme UCH37 to 26S proteasomes

Jun Hamazaki[1,2], Shun-ichiro Iemura[3], Tohru Natsume[3], Hideki Yashiroda[1], Keiji Tanaka[1] and Shigeo Murata[1,4,*]

[1]Laboratory of Frontier Science, Core Technology and Research Center, Tokyo Metropolitan Institute of Medical Science, Bunkyo-ku, Tokyo, Japan, [2]Department of Biological Sciences, Graduate School of Science, Tokyo Metropolitan University, Hachiohji, Tokyo, Japan, [3]National Institutes of Advanced Industrial Science and Technology, Biological Information Research Center, Kohtoh-ku, Tokyo, Japan and [4]PRESTO, Japan Science and Technology Agency, Kawaguchi, Saitama, Japan

The 26S proteasome is a multisubunit protease responsible for regulated proteolysis in eukaryotic cells. It is composed of one catalytic 20S proteasome and two 19S regulatory particles attached on both ends of 20S proteasomes. Here, we describe the identification of Adrm1 as a novel proteasome interacting protein in mammalian cells. Although the overall sequence of Adrm1 has weak homology with the yeast Rpn13, the amino- and carboxyl-terminal regions exhibit significant homology. Therefore, we designated it as hRpn13. hRpn13 interacts with a base subunit Rpn2 via its amino-terminus. The majority of 26S proteasomes contain hRpn13, but a portion of them does not, indicating that hRpn13 is not an integral subunit. Intriguingly, we found that hRpn13 recruits UCH37, a deubiquitinating enzyme known to associate with 26 proteasomes. The carboxyl-terminal regions containing KEKE motifs of both hRpn13 and UCH37 are involved in their physical interaction. Knockdown of hRpn13 caused no obvious proteolytic defect but loss of UCH37 proteins and decrease in deubiquitinating activity of 26S proteasomes. Our results indicate that hRpn13 is essential for the activity of UCH37.

The EMBO Journal (2006) **25,** 4524–4536. doi:10.1038/sj.emboj.7601338; Published online 21 September 2006
Subject Categories: proteins
Keywords: deubiquitinating enzyme; proteasome; Rpn13; ubiquitin; UCH37

Introduction

The ubiquitin–proteasome system is the main non-lysosomal route for intracellular protein degradation in eukaryotes (Glickman and Ciechanover, 2002). Short-lived proteins as well as abnormal proteins in cells are recognized by the ubiquitin system and are marked with ubiquitin chains as a degradation signal. Polyubiquitinated proteins are then recognized and degraded by 26S proteasomes. The 26S proteasome is a huge protein complex of approximately 2.5 MDa composed of one proteolytically active 20S proteasome and two 19S regulatory particles (RP), each attached to one end of the 20S proteasome (Baumeister *et al*, 1998). The 20S proteasome is a barrel-shaped complex formed by the axial stacking of four rings made up of two outer α-rings and two inner β-rings, which are each made up of seven structurally similar α- and β-subunits, respectively, being associated in the order of $\alpha_{1-7}\beta_{1-7}\beta_{1-7}\alpha_{1-7}$ (Coux *et al*, 1996). The interior of the cavity composed of β-rings is responsible for its proteolytic activity. However, the entry of substrates into the cavity of 20S proteasomes is restricted by the narrow gate of α-rings, which is closed in itself. The 19S RP plays an important role in the degradation of ubiquitinated proteins. The 19S RP can be divided into two subcomplexes, known as 'base' and 'lid' (Glickman *et al*, 1998). The base is made up of six ATPases (Rpt1–Rpt6) and two large regulatory components, Rpn1 and Rpn2, functioning as presumptive receptor(s) of ubiquitin-like proteins (Leggett *et al*, 2002), whereas the lid contains multiple non-ATPase subunits (Rpn3, Rpn5–9, Rpn11–13, and Rpn15). The base complex binds to the outer α-ring of the 20S proteasome and opens a narrow gate in an ATP-dependent manner (Smith *et al*, 2005). In addition, the ATPase subunits supply energy for unfolding target proteins, so that they can be translocated into the β-ring cavity of 20S proteasomes where active sites are located. The role of the lid complex is less unraveled. Among the lid subunits, Rpn11 is known as a metalloprotease that cleaves the peptide bonds between the substrate and the most proximal ubiquitin of the polyubiquitin chains (Verma *et al*, 2002; Yao and Cohen, 2002). Rpn10 is thought to lie between the base and the lid complex and serve as one of the ubiquitin receptors (Verma *et al*, 2004).

In addition to the genuine proteasome subunits, several molecules that associate with proteasomes and play auxiliary roles have been identified (Verma *et al*, 2000; Leggett *et al*, 2002). Most of the proteasome studies have been carried out using yeast cells, especially budding yeasts, and less is known about mammalian proteasomes and some of the counterparts of yeast proteasome subunits have not yet been identified. Here, we show that Adrm1, which was previously reported as a membrane glycoprotein (Shimada *et al*, 1991, 1994), is an ortholog of yeast Rpn13 and identify it as a novel interacting protein of mammalian 26S proteasomes. Furthermore, we reveal that it recruits UCH37, a deubiquitinating enzyme (DUB) associated with proteasomes (Lam *et al*, 1997; Li *et al*, 2000; Stone *et al*, 2004).

Results

Adrm1 is a mammalian ortholog of yeast Rpn13

To identify proteins involved with mammalian proteasomes, we searched for cellular proteins that physically associate,

*Corresponding author. Laboratory of Frontier Science, Core Technology and Research Center, Tokyo Metropolitan Institute of Medical Science, 3-18-22 Honkomagome, Bunkyo-ku, Tokyo 113-9613, Japan. Tel./Fax: +81 3 3823 2237; E-mail: smurata@rinshoken.or.jp

Received: 21 February 2006; accepted: 15 August 2006; published online: 21 September 2006

directly or indirectly, with 26S proteasomes in mammalian cells. For this purpose, the human ortholog of Rpn10 (hRpn10: hereafter, 'h' is used as a prefix to indicate a human ortholog of any yeast proteasome subunit) with a carboxyl-terminal Flag tag was expressed in HEK293 cells and immunoprecipitated from cell lysates with anti-Flag antibody. The immunoprecipitates were eluted with Flag peptides, digested with Lys-C endopeptidase, and analyzed using a highly sensitive direct nano-flow liquid chromatography/tandem mass spectrometry (LC–MS/MS) (Natsume *et al*, 2002). Following a database search, 30 peptides were assigned to MS/MS spectra for Flag-hRpn10-associated complexes (Supplementary Figure 1). These data identified almost all the subunits of 26S proteasomes. In addition, we identified a molecule with yet unknown relevance to proteasomes, called Adrm1.

Adrm1 was previously reported as a membrane glycoprotein with a molecular mass of 110 kDa and involved in cell adhesion (Shimada *et al*, 1994; Simins *et al*, 1999; Natsume *et al*, 2002). Exploration of the Proteome BioKnowledge Library (https://www.proteome.com/proteome/Retriever/index.html) database indicated that Adrm1 is weakly homologous to Rpn13, a subunit of budding yeast proteasomes (Verma *et al*, 2000). The overall sequence of Adrm1 showed 24.9% homology with that of Rpn13, whereas it exhibited a high homology of 60.2% with the amino-termini of Adrm1 (residues 22–111) and Rpn13 (residues 7–103). We also identified 74.4% homology between the C-termini of Adrm1 (residues 366–407) and Rpn13 (residues 114–156) (Figure 1). Accordingly, we renamed the molecule hRpn13.

Identification of hRpn13 as a novel proteasome interacting protein in mammals

To verify that hRpn13 is a human counterpart of yeast Rpn13, we tested whether hRpn13 is incorporated into 26S proteasomes. Extracts of 293T cells were fractionated by glycerol gradient centrifugation, and each fraction was subjected to immunoblotting with anti-hRpn13 antibody. Almost all hRpn13 proteins co-sedimented with 26S proteasomes that were detected by succinyl-Leu-Leu-Val-Tyr-7-amido-4-methylcoumarin (Suc-LLVY-MCA)-hydrolyzing activity and sedimentation of a genuine proteasome subunit hRpn1 (Figure 2A). Free forms of hRpn13 were not apparently observed (Figure 2A). 26S proteasomes were further purified from fractions 18–20 by immunoprecipitation using anti-hRpt6 antibody, and then the immunoprecipitates were subjected to two-dimensional polyacrylamide gel electrophoresis (2D-PAGE). Immunoblot for hRpn13 detected a spot that had an isoelectric point (p*I*) and molecular mass that corresponded to the predicted values of p*I* 4.8 and 42.1 kDa, respectively (Figure 2B). Tandem mass spectrometric analysis identified this spot as Adrm1 (data not shown). Adrm1 has been reported as a glycosylated membrane protein with a molecular mass of 110 kDa (Shimada *et al*, 1994), which is in conflict with the notion that Adrm1, that is, hRpn13, is a subunit of proteasomes. Immunostaining of HeLa cells using anti-hRpn13 and anti-hRpn1 antibodies showed that the distribution of hRpn13 was mainly in the nucleus and partially in the cytosol, a pattern quite similar to the distribution of hRpn1 (Figure 2C). These results were in agreement with those reported previously showing that proteasomes are predominantly present in the nuclei of rapidly proliferating mammalian cells (Kumatori *et al*, 1990). Thus, in our hands, there was no evidence that hRpn13 is a membrane protein.

Next, we examined whether all 26S proteasomes contain hRpn13. The 26S proteasome fractions (fractions 18–20 in Figure 2A) were immunodepleted using anti-hRpt6 antibody, anti-hRpn13 antibody, or preimmune serum. Anti-hRpt6 antibody completely immunodepleted hRpn13 and other 19S RP

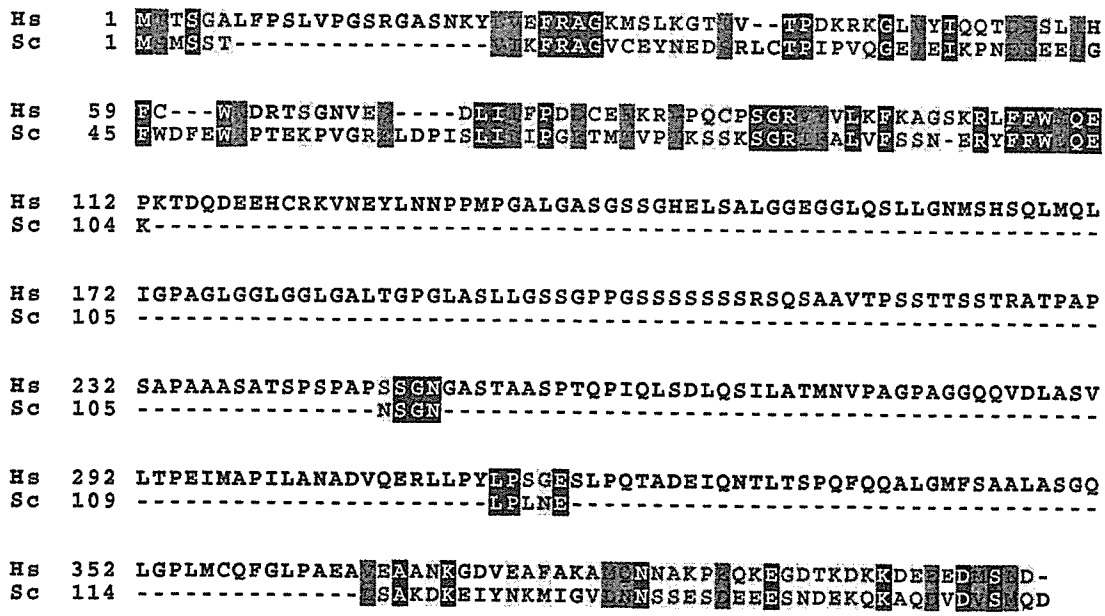

Figure 1 Sequence alignment of human Adrm1 and budding yeast Rpn13. The amino-acid sequences were aligned by the DIALIGN-T program. Amino acids that are identical, strongly similar, and weakly similar between the two sequences are boxed in black, dark gray, and light gray, respectively. Hs: *Homo sapiens*; Sc: *Saccharomyces cerevisiae*.

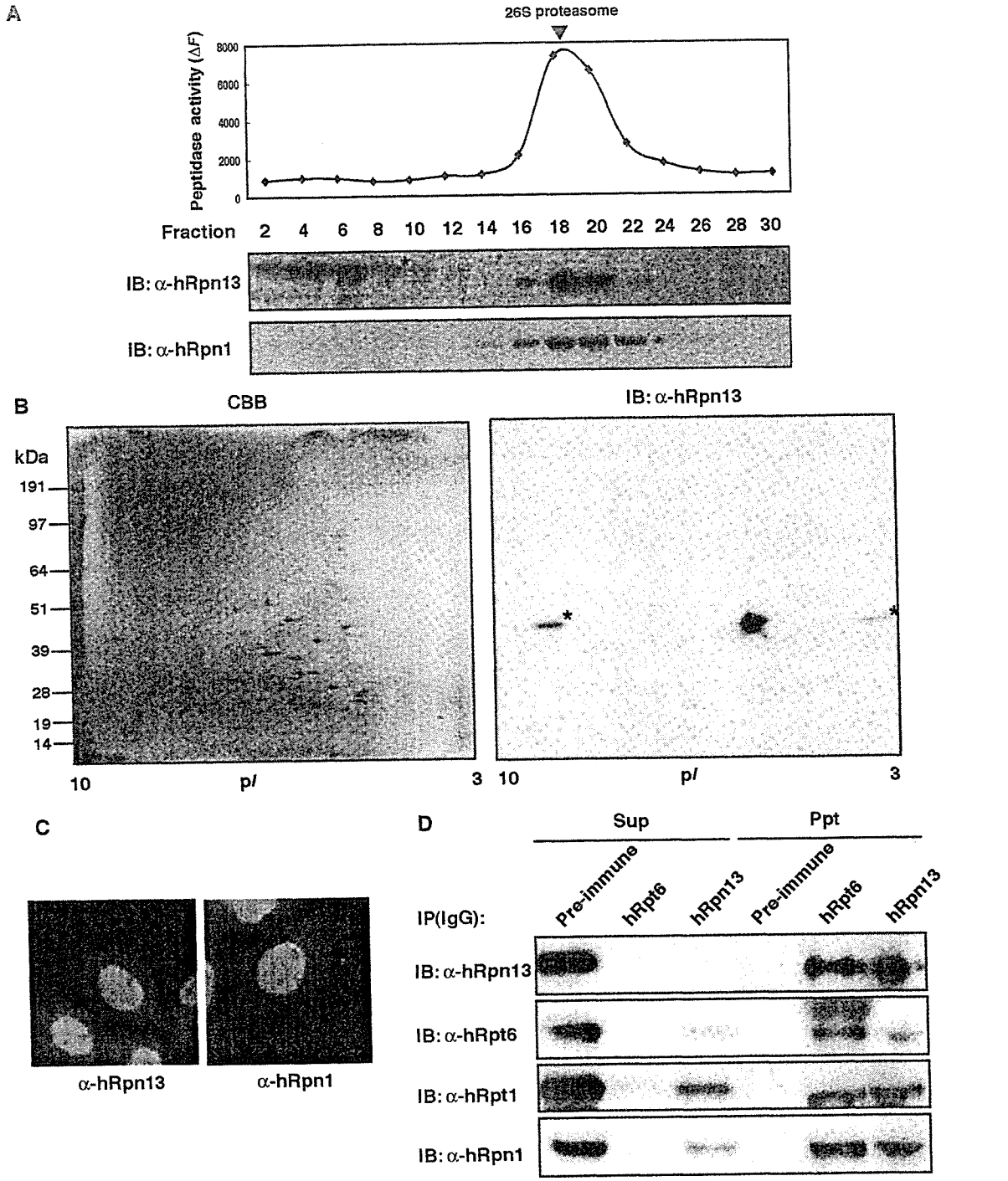

Figure 2 hRpn13 is a subunit of mammalian 26S proteasomes. (**A**) Sedimentation velocity analysis. Extracts of HEK293T cells were fractionated by 10–40% glycerol gradient centrifugation into 32 fractions from the top. An aliquot of each fraction was subjected to the assay of Suc-LLVY-MCA-hydrolyzing activity (upper panel). Immunoblot analysis of each fraction was performed using antibodies against hRpn1 and hRpn13 (lower panels). Arrowhead indicates the peak fraction of 26S proteasomes. Asterisk indicates artifact bands. (**B**) Affinity purification of human proteasomes. Fractions 18–20 in panel A were subjected to immunoprecipitation using anti-hRpt6 antibody. The precipitates were eluted with glycine-HCl and resolved by 2D-PAGE, followed by Coomassie brilliant blue (CBB) staining (left panel) and immunoblot with anti-hRpn13 antibody (right panel). (**C**) Intracellular distribution of hRpn13 in HeLa cells. hRpn13 (left panel) and hRpn1 (right panel) were detected with anti-hRpn13 or anti-hRpn1 antibody and visualized with Alexa488-conjugated anti-rabbit IgG antibody. (**D**) Immunodepletion analysis. Fractions 18–20 in panel A were pooled and immunoprecipitated with anti-hRpt6 antibody, anti-hRpn13 antibody, or preimmune serum. The unbound fractions and immunoprecipitates were subjected to SDS–PAGE, followed by immunoblotting for hRpn13, hRpt6, hRpt1, and hRpn1.

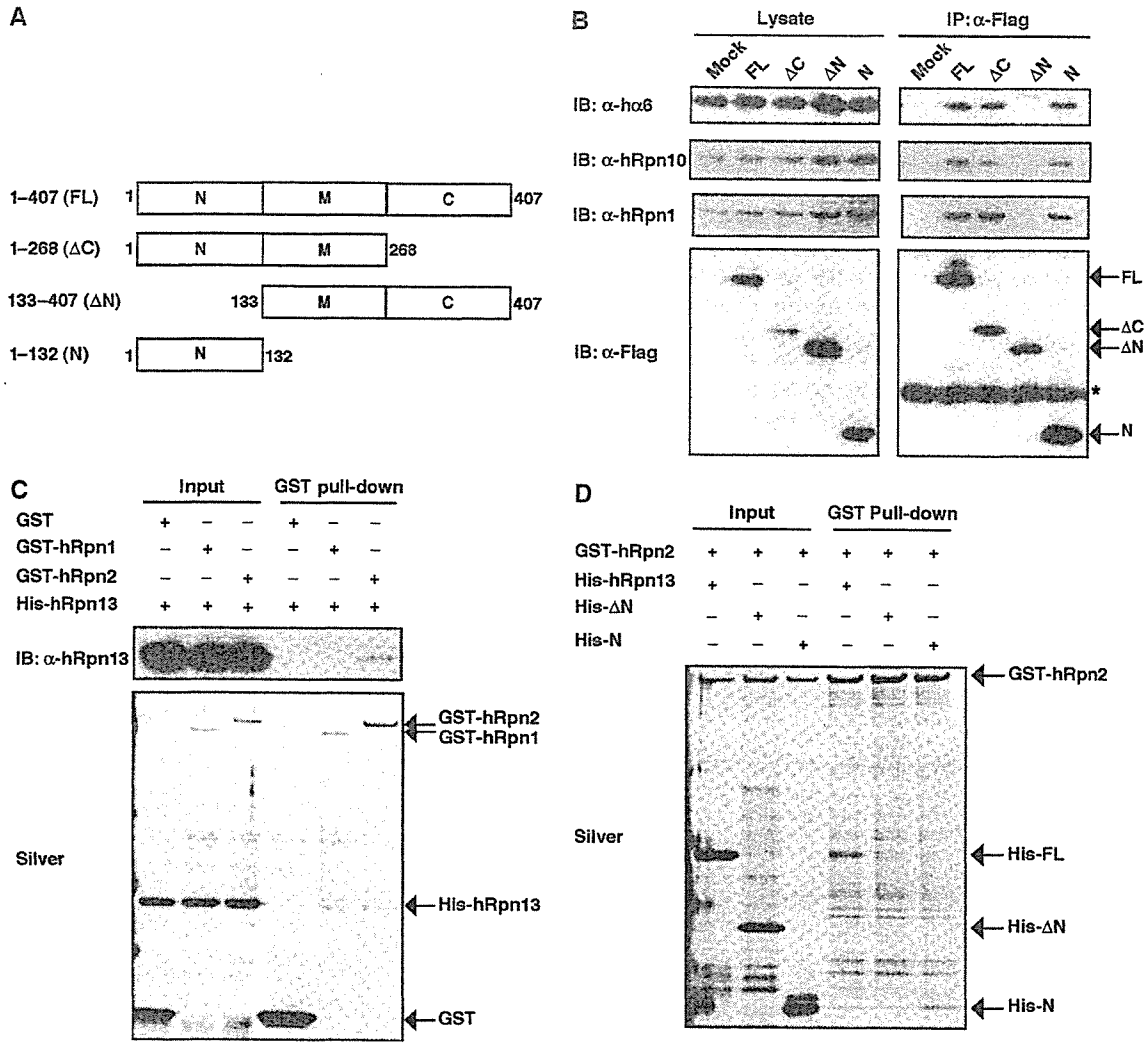

Figure 3 hRpn13 associates with proteasomes via its N-terminal region. (**A**) Schematic representation of constructs for Rpn13 and its dissected mutants used. (**B**) Flag-tagged plasmids encoding hRpn13 and its deletion mutants depicted in panel A were transfected into HEK293T cells. The cell lysates were immunoprecipitated with anti-Flag antibody, followed by immunoblotting for hα6, hRpn10, hRpn1, and Flag epitopes. (**C**) GST pull-down analysis of recombinant proteins. GST, GST-hRpn1, and GST-hRpn2 were incubated with 6xHis-hRpn13 for 1 h at 4°C and then precipitated with glutathione Sepharose. The bound proteins were analyzed by SDS–PAGE, followed by silver staining and immunoblotting with anti-hRpn13 antibody. (**D**) GST pull-down analysis of recombinant proteins. GST-hRpn2 was incubated with 6xHis-hRpn13 or its mutant forms and then pulled down with glutathione Sepharose followed by silver staining.

subunits such as hRpt1 and hRpn1. In contrast, anti-hRpn13 antibody did not remove all the 19S RP subunits, with about 10% input of 19S RP being left in the unbound fraction, whereas it completely depleted hRpn13 (Figure 2D). These results indicate that hRpn13 is incorporated into the majority of 26S proteasomes, but a portion of 26S proteasomes does not contain hRpn13. Therefore, we conclude that hRpn13 is one of the near-stoichiometric proteasome interacting proteins (PIPs), like Ubp6 and Ecm29 in budding yeast (Leggett *et al*, 2002), and is not an integral subunit of 26S proteasomes.

The conserved N-terminal region of hRpn13 is required for association with proteasomes

Based on the sequence alignment, we postulated that hRpn13 is composed of three regions. The N- and C-terminal regions are conserved between budding yeast and human, and the internal region that lies between the N- and C-terminal regions is not found in the budding yeast Rpn13 (Figure 1). We tentatively divided hRpn13 into three portions. The 'N' portion encompassed the conserved N-terminal region (i.e. amino acids 1–132) and the 'C' portion corresponded to amino acids 269–407 that included the conserved C-terminal region. The portion between 'N' and 'C' was designated 'M' portion (Figure 3A). In the next step, we determined the portion required for incorporation into proteasomes. Various deletion constructs encoding wild-type and mutant hRpn13 with Flag tag were expressed in HEK293T cells and immunoprecipitated with anti-Flag antibody. The hRpn13 mutants that lacked the C portion or encoded solely the N portion precipitated various proteasome subunits such as hα6, hRpn10, and hRpn1, as did full-length hRpn13 (Figure 3B). In contrast, hRpn13 that lacked the N portion did not precipitate these subunits (Figure 3B). These results indicate

that the N portion, that is, the conserved N-terminal region of hRpn13, is essential and sufficient for its association with proteasomes.

hRpn13 directly interacts with a base subunit hRpn2

The next set of experiments determined the subunit of 26S proteasomes associated with hRpn13. For this purpose, we tested the interaction between hRpn13 and each subunit of mammalian 19S RP by yeast two-hybrid analysis. The results identified hRpn1 and hRpn2 as possible interacting subunits with hRpn13 (data not shown). Furthermore, comprehensive interactive proteome analysis in budding yeast showed interaction of Rpn13 with Rpn2 (Ito *et al*, 2001). Therefore, we purified recombinant proteins of hRpn1, hRpn2, and hRpn13 and performed *in vitro* binding analysis (Figure 3C). hRpn13 was pulled down by glutathione *S*-transferase (GST)-hRpn2 but not by GST-hRpn1, indicating that hRpn13 is directly associated with hRpn2. Next, we tested whether the N-terminal region of hRpn13 is required for the association with hRpn2. As shown in Figure 3D, the N portion of hRpn13 was required and sufficient for interaction with GST-hRpn2, which was consistent with the results shown in Figure 3B. Based on these results, we conclude that hRpn13 is associated with 26S proteasomes via hRpn2, with which the conserved N-terminal region of hRpn13 interacts.

Knockdown of Rpn13 does not cause proteolytic defects in proteasomes

In budding yeast, deletion of Rpn13 is not lethal, unlike most other proteasome subunits, but causes defect in the degradation of a ubiquitin-fusion-degradation (UFD) substrate (Verma *et al*, 2000). To elucidate the function of hRpn13 in mammalian cells, we knocked down hRpn13 by small interfering RNA (siRNA) in HEK293T cells. As a positive control for proteasome dysfunction, knockdown of hRpt2 was also performed. In hRpt2 knockdown cells, a decrease in hRpt2 protein levels resulted in a concomitant loss of hRpn13 as well as other genuine proteasome subunits such as hRpn1 and hα6. Consequently, hRpt2-knockdown cells showed cell death (data not shown) and accumulation of polyubiquitinated proteins (Figure 4A), which are hallmarks of proteasome dysfunction. These results indicate that hRpt2 is required for the integrity of proteasome structure and function and that hRpn13 is stably expressed in the presence of normal proteasomes. In hRpn13-knockdown cells, the expression of hRpn13 was almost abrogated, but the expression of other proteasome subunits was not changed (Figure 4A). The cells showed normal growth (data not shown) and no accumulation of polyubiquitinated proteins (Figure 4A). These features were in contrast to the phenotypes of hRpt2 knockdown. When the extracts from HEK293T cells were fractionated by glycerol-density gradient centrifugation, an active enzyme that catalyzes the degradation of the fluorogenic substrate Suc-LLVY-AMC was sedimented with a sedimentation coefficient of approximately that of 26S, but low activity was found in the slowly sedimenting fractions corresponding to the sedimentation position of the purified 20S proteasome (Figure 4B, upper panel). The addition of 0.05% SDS, which is a potent artificial activator of the latent 20S proteasome, caused marked activation of the enzyme sedimenting like the 20S proteasome (Figure 4B, lower panel). As shown in Figure 4B, the peptide-hydrolyzing activities of both 20S and 26S proteasomes remained unchanged irrespective of hRpn13 knockdown. Next, we tested the activities of protein degradation *in vitro* (Figure 4C and D) and *in vivo* (Figure 4E). Assay of antizyme (AZ)-dependent ornithine decarboxylase (ODC) degradation, which measures ATP-dependent and ubiquitin-independent proteolytic activity of 26S proteasomes (Murakami *et al*, 1992), did not show decreased proteolytic activity. Rather, the activity was increased 1.4-fold in the hRpn13-knockdown cells (Figure 4C). We also examined ubiquitin-dependent proteolytic activity using *in vitro* ubiquitinated cIAP1 (inhibitor of apoptosis-1), which is a ubiquitin ligase that catalyzes its own ubiquitination for degradation (Yang *et al*, 2000). As shown in Figure 4D, extracts of hRpn13-knockdown cells showed normal proteolytic activity in the degradation of ubiquitinated cIAP1 proteins. IκBα is also a well-known substrate of 26S proteasomes that is rapidly ubiquitinated and degraded in response to TNF-α (Suzuki *et al*, 2000). To check proteasome activities *in vivo*, we monitored the degradation rate of IκBα. hRpn13-knockdown cells showed the same degradation efficiency as control cells (Figure 4E). Considered together, the above results suggest that hRpn13 is not essential for overall protein degradation and viability of mammalian cells.

hRpn13 interacts with UCH37 via its C-terminus

Whereas the N-terminal region of hRpn13 is essential for association with 26S proteasomes (Figure 3), the role of the conserved C-terminal region is still unknown. To elucidate its role, we again used the proteomic approach. Flag-tagged hRpn13ΔN that did not interact with proteasomes (Figure 3) was expressed in HEK293 cells and immunoprecipitated from the cell lysate with anti-Flag antibody, followed by LC–MS/MS analysis. The peptides most abundantly identified were those of UCH37 (also called UCHL5) (Figure 5A), which is reported to be associated with proteasomes in fission yeast, fly, and mammals (Lam *et al*, 1997; Holzl *et al*, 2000; Li *et al*, 2000, 2001; Stone *et al*, 2004). We noticed that both hRpn13 and UCH37 had KEKE motifs at their C-terminal extremities. The conserved C-terminal region of hRpn13 is composed of one typical KEKE at its C-terminus (hereafter referred to as KE2) and one KE-rich region adjacent to KE2, which does not fit the definition of KEKE motif, as proposed previously (Realini *et al*, 1994), but is rich in lysine and glutamic acid residues (hereafter referred to as KE1) (Figure 5B, left panel). A proline residue known as a potent α-helical and β-sheet structure breaker (MacArthur and Thornton, 1991) was located between KE1 and KE2. KEKE motifs are known to mediate protein–protein interactions (Realini *et al*, 1994), and we hypothesized that the interaction between these two molecules was KEKE motif dependent. To test this notion, we expressed Flag-tagged hRpn13, hRpn13ΔKE2 lacking typical KEKE motif, and hRpn13ΔKE1 + 2, which lacked both KE1 and KE2 and thus the entire conserved C-terminal region, in HEK293T cells and immunoprecipitation was achieved with anti-Flag antibody (Figure 5B, right panel). Although the three constructs precipitated nearly the same amount of hα6 and hRpn1, hRpn13ΔKE2 precipitated less amount of UCH37 compared with the wild-type hRpn13, and hRpn13ΔKE1 + 2 did not precipitate UCH37. These results indicate that the conserved C-terminal region is required for the interaction with UHC37.

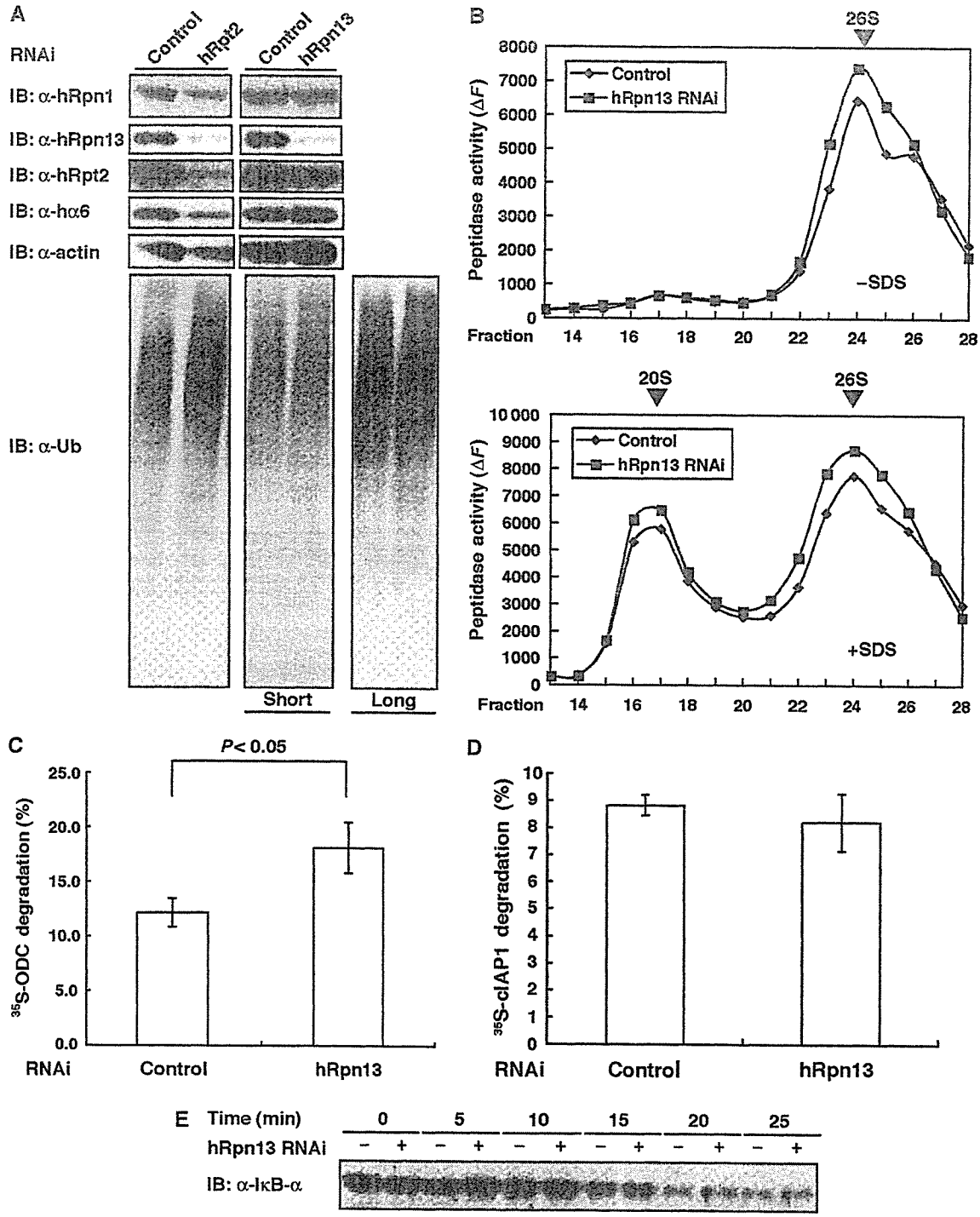

Figure 4 siRNA-mediated knockdown of hRpn13 does not cause proteolytic defects in proteasomes. (**A**) HEK293T cells were transfected with siRNA against hRpn13 or hRpt2. After 48 h for hRpt2 knockdown and 96 h for hRpn13 knockdown, cell extracts were subjected to SDS–PAGE, followed by immunoblotting with the indicated antibodies. (**B**) Extracts of control and Rpn13-knockdown cells were fractionated by 8–32% glycerol gradient centrifugation into 32 fractions from the top. Suc-LLVY-AMC hydrolysis activities were measured in the absence (left) or presence (right) of 0.05% SDS. 20S: 20S proteasome; 26S: 26S proteasome. (**C**) Ubiquitin-independent protein-degrading activity of proteasome. ATP- and AZ-dependent degradation of ^{35}S-labeled ODC protein was assayed. Knockdown cells showed significantly increased activity ($P<0.05$, one-way analysis of variance). Data are mean±s.e.m. values of three independent experiments. (**D**) Ubiquitinated cIAP1-degrading activity of proteasomes. Ubiquitin-dependent degradation of ubiquitinated ^{35}S-labeled cIAP1 was assayed. Data are mean±s.e.m. values of three independent experiments. (**E**) Effect of hRpn13 knockdown on TNF-α-induced degradation of IκBα *in vivo*. HEK293T cells were treated with TNF-α for the indicated times in the presence of cycloheximide. The levels of IκBα proteins were analyzed by immunoblotting.

A

Protein symbol	Protein name	Peptides
UCH37	Ubiquitin carboxy-terminal hydrolase 37	7
TIMM13	Translocase of inner mitochondrial membrane 13 homolog	4
YWHAE	14-3-3 epsilon	4
PRDX1	Peroxiredoxin 1	2
USMG5	Upregulated during skeletal muscle growth 5	2
BUB3	BUB3 budding uninhibited by benzimidazoles 3 homolog	1
TIMM8A	Translocase of inner mitochondrial membrane 8 homolog A	1

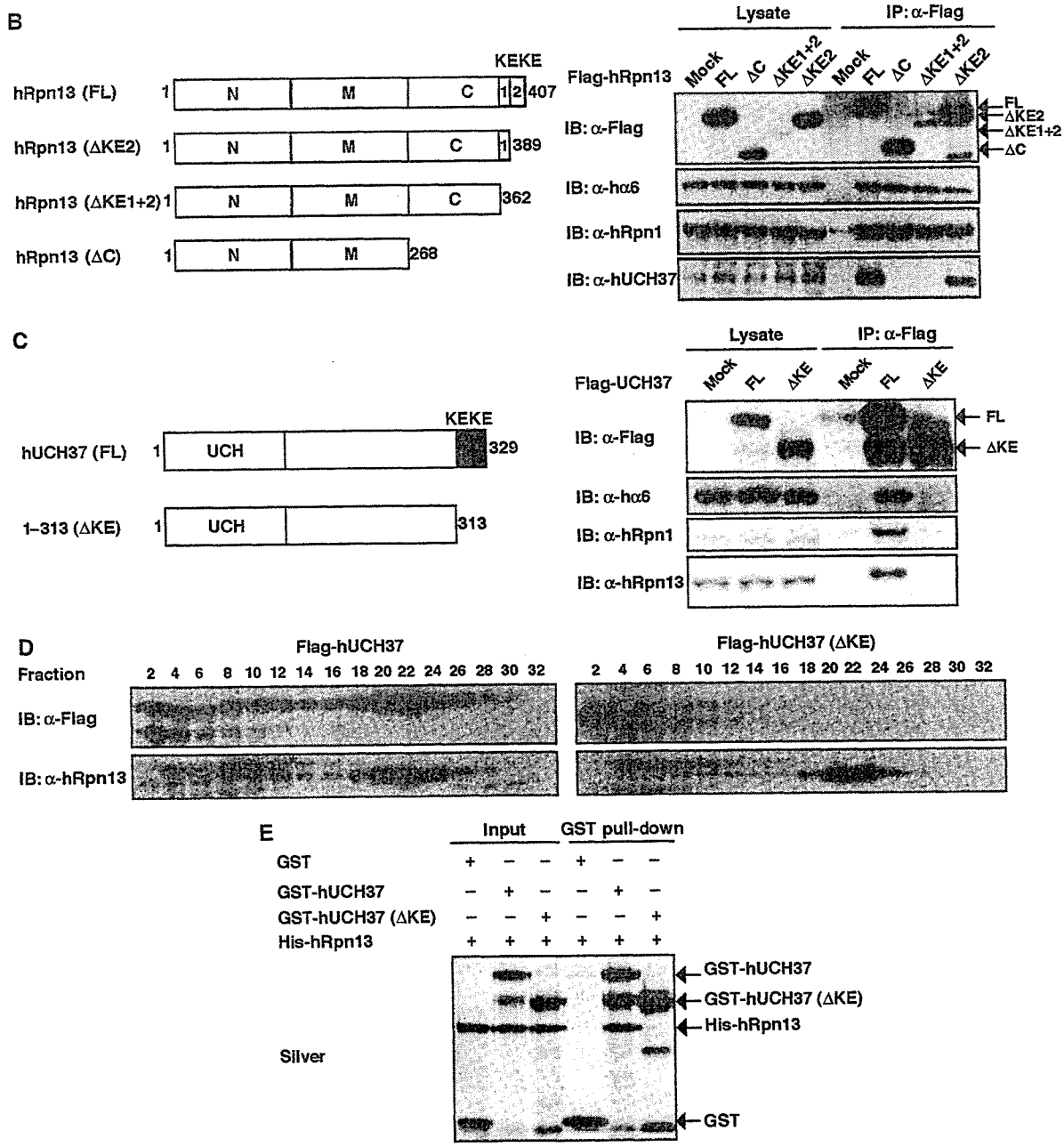

Figure 5 UCH37 interacts with hRpn13. (**A**) A list of proteins detected in four independent hRpn13ΔN immunoprecipitations by LC–MS/MS analysis. The number of identified peptides of each protein is shown. (**B**) Flag-tagged plasmids encoding hRpn13 and its deletion mutants depicted in the left panel were transfected into HEK293T cells. The cell lysates were immunoprecipitated with anti-Flag antibody, followed by immunoblotting for hα6, UCH37, hRpn1, and Flag (right panel). (**C**) Schematic representation of the structures of wild-type UCH37 (FL) and KEKE domain deletion mutant (left panel). HEK293T cells stably expressing Flag-tagged UCH37 (FL), ΔKE, and an empty vector were lysed and subjected to immunoprecipitation with anti-Flag antibody, followed by immunoblot for Flag, hα6, hRpn1, and hRpn13 (right panel). (**D**) The extracts of cells stably expressing Flag-UCH37 and Flag-UCH37ΔKE were fractionated by 10–40% glycerol gradient centrifugation. Immunoblot analysis was performed for each fraction using antibodies against Flag and hRpn13. Asterisks indicate artifact bands. (**E**) GST pull-down analysis of recombinant proteins. GST, GST-UCH37, or GST-ΔKEKE were incubated with 6xHis-Rpn13 and precipitated as in Figure 3C, followed by silver staining.

Next, we examined the role of the KEKE motif of UCH37. As shown in Figure 5C, UCH37 that lacked the KEKE motif (UCH37ΔKE) did not associate with hRpn13 and other proteasome subunits, whereas full-length UCH37 did. Glycerol-density gradient analysis of the extracts showed that a large portion of full-length UCH37 co-sedimented with 26S proteasomes, whereas UCH37ΔKE was observed exclusively in much lighter fractions, presumably as a free form, and that overexpression of UCH37ΔKE did not affect the association of hRpn13 with 26S proteasomes (Figure 5D). In *in vitro* experiments, GST-UCH37 pulled down hRpn13, but GST-UCH37ΔKE did not (Figure 5E), verifying the results depicted in Figure 5C and D. These results indicate that the KEKE motif of UCH37 is necessary for interaction with hRpn13, and hence, with 26S proteasomes.

Knockdown of hRpn13 causes loss of UCH37 proteins

Next, we examined the relationship between hRpn13 and UCH37 in knockdown experiments. We also performed knockdown of USP14, a human ortholog of yeast Ubp6, which is another proteasome-associated DUB (Leggett *et al*, 2002), to examine the relative contributions of UCH37 and USP14 in deubiquitinating activities of 26S proteasomes. Intriguingly, knockdown of hRpn13 caused marked reduction of total cellular UCH37 proteins but not USP14 proteins. On the other hand, knockdown of UCH37 did not affect the level of hRpn13 proteins (Figure 6A). The observed phenotypes of UCH37 knockdown were similar to those of hRpn13 knockdown with regard to cell growth and levels of polyubiquitinated proteins, which were almost the same as the control (Figure 6B and C). Glycerol-density gradient analysis of the extracts of hRpn13-knockdown cells again showed loss of UCH37 proteins in both free and 26S proteasome fractions, with unchanged distributions of proteasome subunits such as hRpn1 and α6 (Figure 6D). Next, we examined the mechanism of decrease in UCH37 proteins in hRpn13-knockdown cells. Control and hRpn13-knockdown cells were treated with various protease inhibitors such as epoxomycin, which is highly specific for proteasomes, MG132, which inhibits both proteasomes and lysosomal enzymes, and E-64d and pepstatin A, which are specific to lysosomal cathepsins. Although these agents worked effectively in inhibiting the relevant proteases (as monitored by the accumulation of polyubiquitinated proteins for proteasome inhibition and accumulation of lipid-conjugated forms of LC3 proteins for inhibition of lysosomal enzymes; Komatsu *et al*, 2005), UCH37 was not increased by any of the inhibitors (Figure 6E). Pulse–chase experiments using HEK293T cells that stably expressed Flag-tagged UCH37 showed almost the same half-life of UCH37 proteins in knockdown cells and control cells (Figure 6F). Semiquantitative reverse transcription–polymerase chain reaction (RT–PCR) showed almost the same expression levels of UCH37 mRNA in hRpn13-knockdown cells and control cells (Figure 6G). Considered together, these results indicate that hRpn13 is required for maintaining normal protein levels of UCH37, and that loss of UCH37 proteins in hRpn13 is not due to metabolic instability of UCH37 proteins or due to repression of transcription of UCH37 mRNA. At present, the mechanism is not clear.

Knockdown of hRpn13 decreases deubiquitinating activities of 26S proteasomes

Finally, we tested the deubiquitinating activities of knockdown cells shown in Figure 6A. As there are abundant DUBs that are not associated with proteasomes, we partially purified complexes of 26S proteasomes and proteasome-associated DUBs by glycerol-density gradient centrifugation, and the 26S proteasome fractions identified by Suc-LLVY-MCA-hydrolyzing activities were used in the following experiments. As shown in Figure 7A, the 26S proteasome fraction of each knockdown cell contained proteasome subunits at a comparable level to each other. Proteins of hRpn13, UCH37, and USP14 were almost completely lost in 26S proteasomes of the cells transfected with siRNAs against hRpn13, UCH37, and USP14, respectively. The deubiquitinating activities of these samples were assayed using ubiquitin-AMC as a substrate. Notably, the deubiquitinating activities of hRpn13- and UCH37-deficient proteasomes were approximately only one-third of those of the control. In contrast, knockdown of USP14 did not significantly reduce the activity. Concomitant knockdown of USP14 with knockdown of hRpn13 or UCH37 did not have additive effects. These results clearly indicate that UCH37 is the dominant DUB associated with mammalian 26S proteasomes and that recruitment of UCH37 by hRpn13 is required for this activity.

Discussion

Adrm1 was originally described as a heavily glycosylated membrane protein of molecular mass 110 kDa (Shimada *et al*, 1991). However, recent studies showed that Adrm1 was hardly, if any, glycosylated and most of it could be detected as a 42 kDa protein (Simins *et al*, 1999; Hasegawa *et al*, 2001; Lamerant and Kieda, 2005). Likewise, the antibody against Adrm1 we raised in this report did not detect the 110 kDa form of Adrm1. Moreover, immunocytochemical analysis of HeLa cells using this antibody indicated that Adrm1 is a soluble protein distributed both in the cytosol and nucleus, which is quite similar to the distribution of proteasomes, as revealed by staining for hRpn1 (Figure 1). Database search analysis suggested that Adrm1 is a human ortholog of yeast Rpn13 subunit. Indeed, Adrm1 was identified in the purified 26S proteasomes at nearly stoichiometric amount, and so we designated it hRpn13. While this manuscript was in preparation, Jorgensen *et al* (2006) reported Adrm1 as a novel proteasome-associated factor (Jorgensen *et al*, 2006). We also identified hRpn2 as an hRpn13-interacting subunit (Figure 3). A previous report mapped the location of p37A (*Drosophila* ortholog of UCH37) in *Drosophila* 26S proteasomes to the interface between the base and the lid, by electron microscopy using gold-labeled ubiquitin-aldehyde bound to the p37A/UCH37 (Holzl *et al*, 2000), which is consistent with our results.

However, immunodepletion analysis showed that not all the 26S proteasomes contain hRpn13 (Figure 2D). In this regard, it is better not to call hRpn13 a subunit of proteasomes but rather regard it as one of the PIPs. Even in yeast, there is no definite evidence to indicate that Rpn13 is a constitutive subunit of proteasomes. In a quantitative mass spectrometric analysis of budding yeast 26S proteasomes, Rpn13 was identified by much smaller number of peptides, compared to authentic proteasome subunits (Guerrero *et al*,

2006). The relatively low homology between Adrm1 and yeast Rpn13 may reflect this fact, as genuine proteasome subunits, but not PIPs, have much higher similarities between human and yeast subunits. Knockdown experiments further revealed that hRpn13 is not essential for proteolysis or viability of mammalian cells, whereas knockdown of hRpt2, a 19S ATPase subunit, was fatal (Figure 4). It is noteworthy that all subunits of RP, except Rpn9, Rpn10,

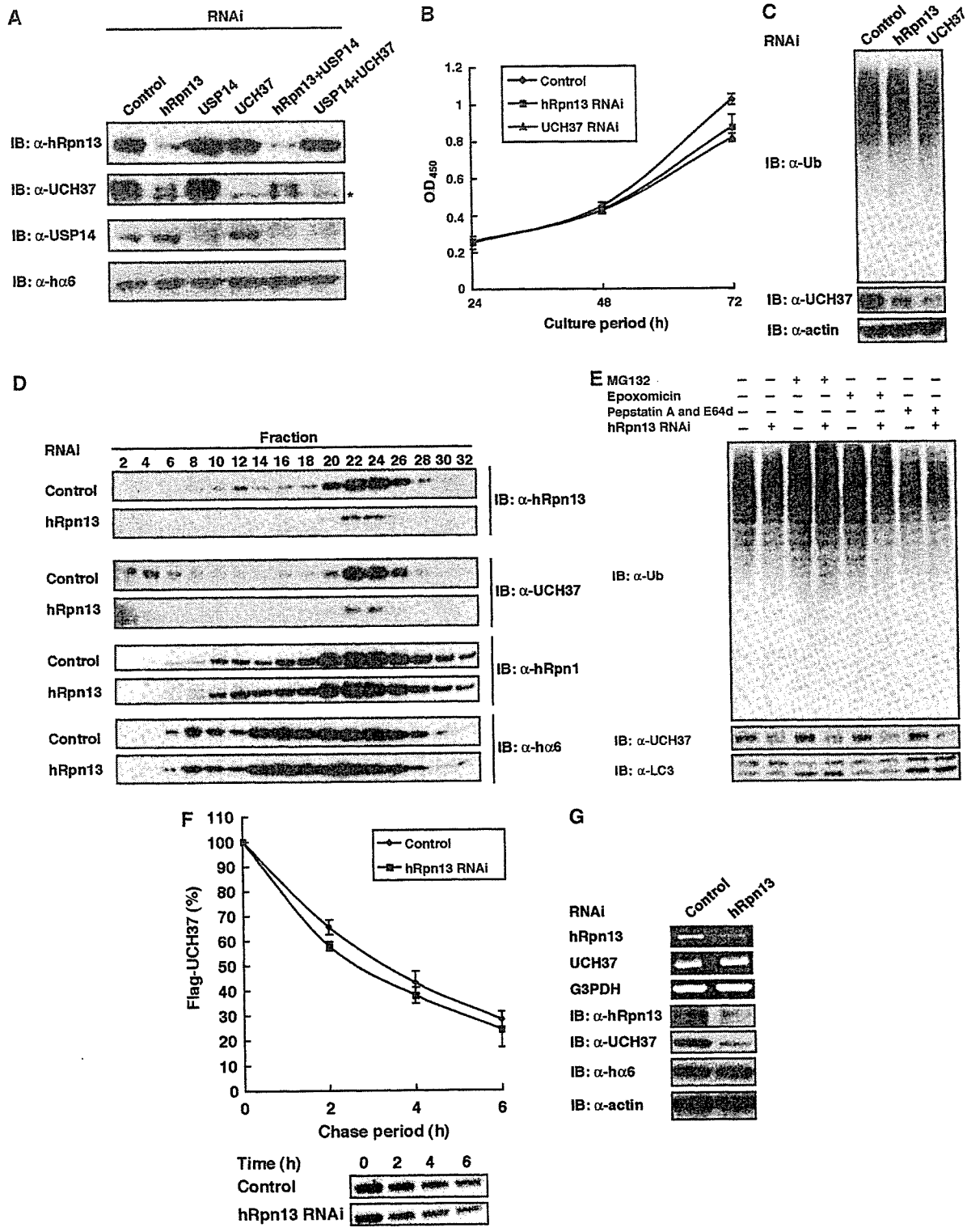

and Rpn15/Sem1, are essential for proliferation of the budding yeast examined so far. Considered together, these results suggest that hRpn13 plays an auxiliary role in the proteasome-dependent protein degradation.

hRpn13 has no known functional motifs and does not seem to be necessary for the structural integrity of proteasomes. Then, what is the role of hRpn13 in proteasomes? hRpn13 can be divided into three functional regions: the N-terminal, C-terminal, and the inserted regions. The former two regions are well conserved from budding yeast to human, whereas the latter one is not found in budding yeast (Figure 1). We proved that the conserved N-terminal region is required for association with proteasomes (Figure 3). We also examined the biological role of the C-terminal region, and our results revealed that it serves as an acceptor for UCH37 (Figure 5). Moreover, loss of hRpn13 proteins caused concurrent loss of UCH37 proteins, indicating that hRpn13 recruits UCH37 to proteasomes and at the same time it is required for maintenance of UCH37 protein levels (Figure 6). As the half-life of UCH37 protein in hRpn13-knockdown cells was similar to that of control cell, the role of hRpn13 in maintaining UHC37 protein levels does not seem to be the stabilization of UCH37 protein. Consistent with this notion, neither the use of a proteasome inhibitor nor a lysosomal inhibitor resulted in accumulation of UCH37 proteins in knockdown cells. The amount of UCH37 mRNA was also unaltered in knockdown cells. At present, we do not know the reason for loss of UCH37 protein in knockdown cells, and the role of the insertion region is yet to be determined. No ortholog of UCH37 is found in budding yeast. Evolutionarily, UCH37 orthologs have emerged synchronously with the insertion region of Rpn13 orthologs. This region may have some role in the relationship with UCH37 and/or other proteins yet to be identified.

Ubp6 (USP14 in mammals) is another well-known DUB that associates with proteasomes. A mutation in USP14 in mice causes neurological disorders, demonstrating the importance of USP14 in mammals. Low expression of USP14 in mice is associated with reduced levels of free ubiquitin, suggesting its role in recycling ubiquitins (Anderson *et al*, 2005), as is also suggested in studies in budding yeast (Guterman and Glickman, 2004). However, the deubiquitinating activity of proteasomes is mainly attributed to UCH37 in fission yeast (Stone *et al*, 2004). Our present study also demonstrates that the deubiquitinating activities of 26S proteasomes are affected more profoundly by loss of UCH37 than USP14, indicating that UCH37 is the dominant DUB over USP14 in mammalian proteasomes. Recruitment of UCH37 by hRpn13 is essential for the activity of UCH37, as hRpn13 knockdown resulted in loss of UCH37, followed by a decrease in the deubiquitinating activity of 26S proteasomes at a level comparable to UCH37 knockdown. Further studies are required to distinguish the roles of USP14 (Ubp6) and UCH37 in organisms that have both molecules. It is plausible that the two molecules have distinct roles.

Despite the significant reduction of deubiquitinating activity of hRpn13-deficient proteasomes, they efficiently

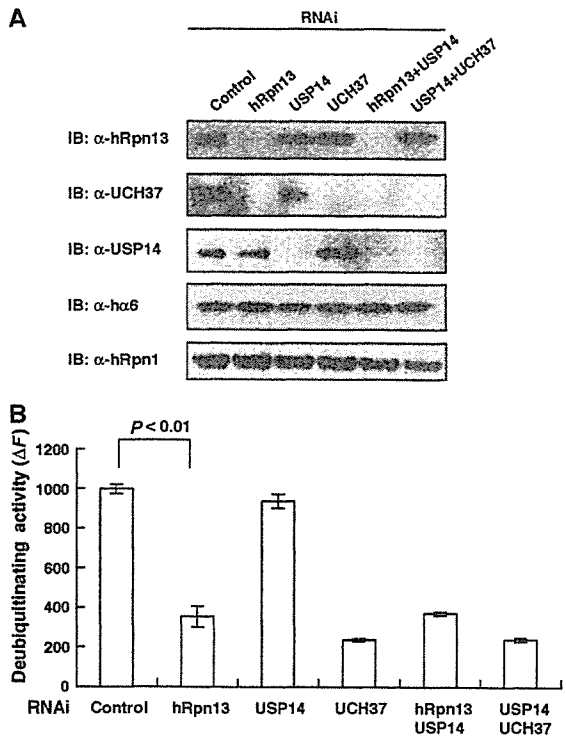

Figure 7 Knockdown of hRpn13 reduces deubiquitinating activities of 26S proteasomes. (**A**) hRpn13 and proteasome associating DUBs in knockdown cells. Cell extracts shown in Figure 6A were fractionated by 10–40% glycerol gradient centrifugation into 32 fractions. Immunoblot analysis of 26S proteasome fractions determined by Suc-LLVY-hydrolyzing activity was performed using the indicated antibodies. (**B**) The deubiquitinating activities of 26S proteasome fractions shown in panel A were measured using ubiquitin-AMC as a substrate. hRpn13- and UCH37-knockdown cells showed significantly reduced deubiquitinating activities ($P<0.01$). Data are mean±s.e.m. values of three independent experiments.

Figure 6 Knockdown of hRpn13 causes loss of UCH37 proteins. (**A**) HEK293T cells were transfected with siRNA against hRpn13, UCH37, or USP14. Where indicated, cells were transfected with a mixture of siRNAs. After 96 h, cell extracts were subjected to SDS–PAGE, followed by immunoblotting with the indicated antibodies. (**B**) Growth rates of hRpn13 knockdown, UCH37 knockdown, and mock cells. The cells were seeded in triplicate in 96-well dishes on day 0 (72 h after transfection), cultured in normal growing medium, and their proliferation was measured every 24 h. Data are mean±s.d. values. (**C**) Cell extracts of hRpn13 knockdown, UCH37 knockdown, and mock cells were subjected to SDS–PAGE, followed by immunoblotting with the indicated antibodies. (**D**) Samples fractionated by 10–40% glycerol gradient centrifugation were immunoblotted with the indicated antibodies. (**E**) Lack of accumulation of UCH37 proteins in hRpn13-knockdown cells following inhibition of the proteasome or lysosomal cathepsins. HEK293T cells transfected with siRNA were treated with MG132 (50 μM, 2 h), epoxomycin (1 μM, 12 h), or E-64 and pepstatin A (10 μg/ml, 12 h). The cells were lysed and subjected to immunoblot. (**F**) Pulse–chase analysis of Flag-UCH37. HEK293T cells stably expressing Flag-UCH37 were pulse-labeled for 30 min with ^{35}S-labeled methionine and chased for the indicated time periods. After immunoprecipitation with M2 agarose, samples were separated by SDS–PAGE and autoradiographed (bottom panels). The upper panel shows the results of band quantitative analysis. Data are mean±s.d. values of three independent experiments. (**G**) hRpn13 knockdown does not alter UCH37 mRNA transcription. Semiquantitative RT–PCR (the upper three panels) and immunoblotting (the lower three panels) were performed using total RNA and proteins extracted from control and hRpn13-knockdown cells 48 h after transfection with siRNAs.

degraded substrate proteins such as ODC, ubiquitinated c-IAP, and IκBα (Figure 4). These observations seem to be in marked contrast to the case of yeast Rpn13, whose deletion caused a complete defect in degradation of a UFD substrate (Verma *et al*, 2000). However, as yeasts that lack Rpn13 are viable (Winzeler *et al*, 1999), the proteolytic defect is probably specific to UFD substrates. Rpn13 may recruit a component essential for degradation of UFD substrates in yeast. The precise role of hRpn13 and UCH37 still remains elusive. Curiously, knockdown of hRpn13 significantly increased the degrading activity of ODC but not that of ubiquitinated cIAP1 protein *in vitro* and IκBα *in vivo*. As sole knockdown of UCH37 did not increase the degrading activity of ODC (data not shown), the results observed in hRpn13 knockdown are not simply due to loss of UCH37. hRpn13 may influence access of protein to the channel of ATPase rings of proteasomes by sitting in the space between the base and lid (Holzl *et al*, 2000), or may recruit proteins that are relevant to proteolysis other than UCH37. At least from these results, both hRpn13 and UCH37 do not seem to be generally required for protein degradation by 26S proteasomes. It is assumed that UCH37 disassembles polyubiquitin chains from the distal end, shortening it such that the attached proteins can be released from the proteasome if there is a delay in efficient degradation (Stone *et al*, 2004). hRpn13 and UCH37 may be important in some specific situations. Further studies are required to determine the specific functions of hRpn13 and UCH37.

Materials and methods

Plasmids and cloning

The complementary DNAs (cDNAs) used in the present study were obtained by RT–PCR from total RNA isolated from HeLa cells or mouse livers using Superscript III (Invitrogen, San Diego, CA) and Pyrobest DNA polymerase (Takara Shuzo, Ohtsu, Japan). All amplified fragments were cloned into pcDNA3.1 vector (Invitrogen) and sequenced for confirmation. Deletion mutants (hRpn13ΔC, ΔN, N, ΔKE1 and ΔKE1 + 2, and UCH37ΔKE) were generated by PCR from wild-type hRpn13 and UCH37 and the Flag tag was introduced at the N-terminus of the constructs. For expression of GST and 6xHis fusion proteins, the cDNAs were subcloned into pGEX6P-1 (Amersham Life Science, Buckinghamshire, UK) and pET-28a (Novagen, Madison, WI) vector, respectively.

Immunological analysis

For immunoprecipitation analysis, HEK293T cells were transfected with plasmids using Fugene 6 (Roche, Mannheim, Germany). After 36 h, the cells were lysed with ice-cold phosphate-buffered saline (PBS) containing 1% Nonidet P-40 (NP-40) and centrifuged at 20 000 *g* for 10 min at 4°C. The supernatant was added with M2-agarose (Sigma Chemical Co., St Louis, MO) and rotated for 1 h at 4°C. The immunoprecipitates were washed five times with ice-cold PBS containing 0.5% NP-40 and then boiled in SDS sample buffer in the presence of β-mercaptoethanol (β-ME). Samples were subjected to SDS–PAGE, transferred to polyvinylidene fluoride membrane, and analyzed by immunoblotting with anti-Flag (M2; Sigma). Polyclonal antibodies against hRpn1, hRpn10, hRpt2, hRpn13, UCH37, and USP14 were raised in rabbits using recombinant proteins expressed in and purified from BL21RIL strain (Novagen) as GST fusion proteins: mouse Rpn1 (full length), mouse Rpn10 (residues 1–251), hRpt2 (residues 1–82), hRpn13 (residues 361–407), mouse UCH37 (residues 228–329), and human USP14 (full length). Anti-LC3 antibody was described previously (Komatsu *et al*, 2005). The antibodies for polyubiquitin and actin were purchased (FK2; MBL, Ina, Japan, Chemicon International Inc., Temecula, CA). All experimental protocols described in this study were approved by the Ethics Review Committee for Animal Experimentation of Tokyo Metropolitan Institute of Medical Science.

GST pull-down assay

Recombinant GST- or 6xHis-tagged proteins were produced in *Escherichia coli* and purified with glutathione Sepharose 4B (Amersham) or Ni-NTA Sepharose (Qiagen, Hilden, Germany). After elution of proteins from the beads, the preparations were dialyzed against buffer A (50 mM Tris–HCl (pH 7.5), 150 mM NaCl, 5 mM β-ME, and 10% glycerol). In GST pull-down analysis, 5 μg of each sample was mixed in 600 μl of buffer A and constantly rotated for 1 h at 4°C, and then 30 μl of glutathione Sepharose 4B was added and further rotated for 1 h. After washing with buffer A, bound proteins were eluted with 10 mM glutathione and subjected to SDS–PAGE, followed by immunoblot and silver staining (Wako Pure Chemical Industries, Osaka, Japan).

RNAi experiments

siRNAs targeting hRpt2, hRpn13, UCH37, and USP14 with the following 25-nucleotide sequences were purchased from Invitrogen: Rpt2, 5′-GGAGUACGAUGUGUAAGUGCCCAUU-3′; Rpn13, 5′-GGA GGGUCUACGUGCUGAAGUUCAAA-3′; UCH37, 5′-ACCGAGCTCAT TAAAGGATTCGGTT-3′; USP14, 5′-UCAGCAUCGUAACACCAGAA GAUAU-3′. siRNAs were transfected into HEK293T cells with Lipofectamine 2000 (Invitrogen) at a final concentration of 2 nM in six-well dishes. The cells were analyzed 96 h (hRpn13, UCH37, USP14, hRpn13 + USP14, and USP14 + UCH37) or 48 h (hRpt2) after transfection. For protease inhibition assay, HEK293T cells transfected with siRNA (96 h) were cultured in the presence or absence of protease inhibitors (50 μM MG132 for 2 h, 10 μg/ml E64d and 10 μg/ml pepstatin A for 12 h, or 1 μM epoxomycin for 12 h). Cell growth was measured using Cell Counting Kit-8 (Wako) according to the instructions provided by the manufacturer. Briefly, cells were seeded at 1×10^3 cells/well in 96-well plates. Absorbance was measured using Microplate reader (Bio-Rad).

Glycerol-density gradient analysis

Mouse livers were homogenized in a Potter-Elvehjem Homogenizer in buffer B (in mM, 25 Tris–HCl (pH 7.5), 2 ATP, 5 $MgCl_2$, and 1 dithiothreitol). HEK293T cells were lysed in buffer B containing 0.2% NP-40. The homogenates and lysates were clarified by centrifugation at 20 000 *g* and subjected to 10–40% (v/v) or 8–32% (v/v) linear glycerol-density density gradient centrifugation (22 h, 83 000 *g*) as described previously (Hirano *et al*, 2005).

In vitro assay of proteasome activity

Proteasome peptidase activity was measured using a peptide substrate, succinyl-Leu-Leu-Val-Tyr-7-amino-4-methyl-coumarin (Suc-LLVY-MCA), and the degradation of the recombinant ^{35}S-labeled ODC was assayed in the presence of ATP, an ATP-regenerating system, and AZ, as described previously (Hirano *et al*, 2005). For the assay of cIAP1 degradation, cDNAs encoding Flag-cIAP1 subcloned into pcDNA3.1 were transcribed *in vitro*, translated, and radiolabeled as described previously (Hirano *et al*, 2005). The ^{35}S-labeled Flag-cIAP1 was purified using M2-agarose (Sigma) and eluted with Flag-peptide (Sigma). For ubiquitination of cIAP1, 3 000 000 c.p.m. of ^{35}S-labeled cIAP1, 0.25 μg of E1, 0.9 μg of UbcH5, and 33 μg of ubiquitin (Sigma) were mixed and incubated in a volume of 80 μl for 90 min at 30°C, as described previously (Murata *et al*, 2001). Finally, 2.5 μl of the ubiquitination mixture was added to 10 μl of cell lysates in the presence of 2 mM ATP, incubated at 37°C for 20 min, and then radioactivities of trichloroacetic acid-soluble fractions were measured.

TNF-α-dependent IκBα degradation

HEK293T cells transfected with siRNA were treated with 100 μg/ml cycloheximide (Sigma) for 10 min, and then human TNF-α (Genzyme, Cambridge, MA) was added at a final concentration of 10 ng/ml. Changes in the protein levels of endogenous IκBα after treatment with TNF-α were analyzed by immunoblotting with anti-IκBα (c-21) (Santa Cruz Biotechnology, Santa Cruz, CA).

Deubiquitination assay

For ubiquitin-7-amino-4-methylcoumarin (ubiquitin-AMC) (Boston Biochem) hydrolysis assays, 10 μl of 26S proteasome fraction separated by glycerol gradient centrifugation was incubated with 0.25 μM ubiquitin-AMC for 15 min at 37°C. The release of AMC was measured fluorometrically.

Pulse–chase analysis

HEK293T cells stably expressing Flag-UCH37 were transfected with siRNA for hRpn13 or control siRNA. Pulse–chase experiments were performed as described previously (Hirano *et al*, 2005).

RT–PCR analysis

Total RNA (2.5 μg) was reverse transcribed using SuperScript III (Invitrogen) and oligo(dT)$_{20}$ primers. Specific primers for each gene were as follows: 5′-AAGGATCCATGAGCATCCTGGCCACG ATGAACG-3′ and 5′-TTCTCGAGTCAGTCCAGGCTCATGTCCTCC-3′ for hRpn13, 5′-AAGGATCCATGACGGGCAACGCCGGGGAG-3′ and 5′-TTCTCGAGTCATTTGGTTTCCTGAGCTTTC-3′ for UCH37, and 5′-ACCACAGTCCATGCCATCAC-3′ and 5′-TCCACCACCCTGTTGCT GTA-3′ for G3PDH.

Supplementary data

Supplementary data are available at *The EMBO Journal* Online (http://www.embojournal.org).

Acknowledgements

We thank Y Murakami for providing the ODC degradation assay system and K Furuyama for technical support. This work was supported in part by a grant to SM from JST and grants to SM and KT from the Ministry of Education, Science and Culture of Japan.

References

Anderson C, Crimmins S, Wilson JA, Korbel GA, Ploegh HL, Wilson SM (2005) Loss of Usp14 results in reduced levels of ubiquitin in ataxia mice. *J Neurochem* **95:** 724–731

Baumeister W, Walz J, Zuhl F, Seemuller E (1998) The proteasome: paradigm of a self-compartmentalizing protease. *Cell* **92:** 367–380

Coux O, Tanaka K, Goldberg AL (1996) Structure and functions of the 20S and 26S proteasomes. *Annu Rev Biochem* **65:** 801–847

Glickman MH, Ciechanover A (2002) The ubiquitin-proteasome proteolytic pathway: destruction for the sake of construction. *Physiol Rev* **82:** 373–428

Glickman MH, Rubin DM, Coux O, Wefes I, Pfeifer G, Cjeka Z, Baumeister W, Fried VA, Finley D (1998) A subcomplex of the proteasome regulatory particle required for ubiquitin-conjugate degradation and related to the COP9-signalosome and eIF3. *Cell* **94:** 615–623

Guerrero C, Tagwerker C, Kaiser P, Huang L (2006) An integrated mass spectrometry-based proteomic approach. *Mol Cell Proteomics* **5:** 366–378

Guterman A, Glickman MH (2004) Complementary roles for Rpn11 and Ubp6 in deubiquitination and proteolysis by the proteasome. *J Biol Chem* **279:** 1729–1738

Hasegawa K, Sakurai N, Kinoshita T (2001) Xoom is maternally stored and functions as a transmembrane protein for gastrulation movement in *Xenopus* embryos. *Dev Growth Differ* **43:** 25–31

Hirano Y, Hendil KB, Yashiroda H, Iemura S, Nagane R, Hioki Y, Natsume T, Tanaka K, Murata S (2005) A heterodimeric complex that promotes the assembly of mammalian 20S proteasomes. *Nature* **437:** 1381–1385

Holzl H, Kapelari B, Kellermann J, Seemuller E, Sumegi M, Udvardy A, Medalia O, Sperling J, Muller SA, Engel A, Baumeister W (2000) The regulatory complex of *Drosophila melanogaster* 26S proteasomes. Subunit composition and localization of a deubiquitylating enzyme. *J Cell Biol* **150:** 119–130

Ito T, Chiba T, Ozawa R, Yoshida M, Hattori M, Sakaki Y (2001) A comprehensive two-hybrid analysis to explore the yeast protein interactome. *Proc Natl Acad Sci USA* **98:** 4569–4574

Jorgensen JP, Lauridsen AM, Kristensen P, Dissing K, Johnsen AH, Hendil KB, Hartmann-Petersen R (2006) Adrm1, a putative adhesion regulating protein, is a novel proteasome-associated factor. *J Mol Biol* **360:** 1043–1052

Komatsu M, Waguri S, Ueno T, Iwata J, Murata S, Tanida I, Ezaki J, Mizushima N, Ohsumi Y, Uchiyama Y, Kominami E, Tanaka K, Chiba T (2005) Impairment of starvation-induced and constitutive autophagy in Atg7-deficient mice. *J Cell Biol* **169:** 425–434

Kumatori A, Tanaka K, Inamura N, Sone S, Ogura T, Matsumoto T, Tachikawa T, Shin S, Ichihara A (1990) Abnormally high expression of proteasomes in human leukemic cells. *Proc Natl Acad Sci USA* **87:** 7071–7075

Lam YA, Xu W, DeMartino GN, Cohen RE (1997) Editing of ubiquitin conjugates by an isopeptidase in the 26S proteasome. *Nature* **385:** 737–740

Lamerant N, Kieda C (2005) Adhesion properties of adhesion-regulating molecule 1 protein on endothelial cells. *FEBS J* **272:** 1833–1844

Leggett DS, Hanna J, Borodovsky A, Crosas B, Schmidt M, Baker RT, Walz T, Ploegh H, Finley D (2002) Multiple associated proteins regulate proteasome structure and function. *Mol Cell* **10:** 495–507

Li T, Duan W, Yang H, Lee MK, Bte Mustafa F, Lee BH, Teo TS (2001) Identification of two proteins, S14 and UIP1, that interact with UCH37. *FEBS Lett* **488:** 201–205

Li T, Naqvi NI, Yang H, Teo TS (2000) Identification of a 26S proteasome-associated UCH in fission yeast. *Biochem Biophys Res Commun* **272:** 270–275

MacArthur MW, Thornton JM (1991) Influence of proline residues on protein conformation. *J Mol Biol* **218:** 397–412

Murakami Y, Matsufuji S, Kameji T, Hayashi S, Igarashi K, Tamura T, Tanaka K, Ichihara A (1992) Ornithine decarboxylase is degraded by the 26S proteasome without ubiquitination. *Nature* **360:** 597–599

Murata S, Minami Y, Minami M, Chiba T, Tanaka K (2001) CHIP is a chaperone-dependent E3 ligase that ubiquitylates unfolded protein. *EMBO Rep* **2:** 1133–1138

Natsume T, Yamauchi Y, Nakayama H, Shinkawa T, Yanagida M, Takahashi N, Isobe T (2002) A direct nanoflow liquid chromatography-tandem mass spectrometry system for interaction proteomics. *Anal Chem* **74:** 4725–4733

Realini C, Rogers SW, Rechsteiner M (1994) KEKE motifs. Proposed roles in protein–protein association and presentation of peptides by MHC class I receptors. *FEBS Lett* **348:** 109–113

Shimada S, Ogawa M, Schlom J, Greiner JW (1991) Identification of a novel tumor-associated Mr 110 000 gene product in human gastric carcinoma cells that is immunologically related to carcinoembryonic antigen. *Cancer Res* **51:** 5694–5703

Shimada S, Ogawa M, Takahashi M, Schlom J, Greiner JW (1994) Molecular cloning and characterization of the complementary DNA of an M(r) 110 000 antigen expressed by human gastric carcinoma cells and upregulated by gamma-interferon. *Cancer Res* **54:** 3831–3836

Simins AB, Weighardt H, Weidner KM, Weidle UH, Holzmann B (1999) Functional cloning of ARM-1, an adhesion-regulating molecule upregulated in metastatic tumor cells. *Clin Exp Metast* **17:** 641–648

Smith DM, Kafri G, Cheng Y, Ng D, Walz T, Goldberg AL (2005) ATP binding to PAN or the 26S ATPases causes association with the 20S proteasome, gate opening, and translocation of unfolded proteins. *Mol Cell* **20:** 687–698

Stone M, Hartmann-Petersen R, Seeger M, Bech-Otschir D, Wallace M, Gordon C (2004) Uch2/Uch37 is the major deubiquitinating enzyme associated with the 26S proteasome in fission yeast. *J Mol Biol* **344:** 697–706

Suzuki H, Chiba T, Suzuki T, Fujita T, Ikenoue T, Omata M, Furuichi K, Shikama H, Tanaka K (2000) Homodimer of two F-box proteins βTrCP1 or βTrCP2 binds to IκBα for signal-dependent ubiquitination. *J Biol Chem* **275:** 2877–2884

Verma R, Aravind L, Oania R, McDonald WH, Yates III JR, Koonin EV, Deshaies RJ (2002) Role of Rpn11 metalloprotease in deubiquitination and degradation by the 26S proteasome. *Science* **298:** 611–615

Verma R, Chen S, Feldman R, Schieltz D, Yates J, Dohmen J, Deshaies RJ (2000) Proteasomal proteomics: identification of nucleotide-sensitive proteasome-interacting proteins by mass spectrometric analysis of affinity-purified proteasomes. *Mol Biol Cell* **11:** 3425–3439

Verma R, Oania R, Graumann J, Deshaies RJ (2004) Multiubiquitin chain receptors define a layer of substrate selectivity in the ubiquitin-proteasome system. *Cell* **118:** 99–110

Winzeler EA, Shoemaker DD, Astromoff A, Liang H, Anderson K, Andre B, Bangham R, Benito R, Boeke JD, Bussey H, Chu AM, Connelly C, Davis K, Dietrich F, Dow SW, El Bakkoury M, Foury F, Friend SH, Gentalen E, Giaever G, Hegemann JH, Jones T, Laub M, Liao H, Liebundguth N, Lockhart DJ, Lucau-Danila A, Lussier M, M'Rabet N, Menard P, Mittmann M, Pai C, Rebischung C, Revuelta JL, Riles L, Roberts CJ, Ross-MacDonald P, Scherens B, Snyder M, Sookhai-Mahadeo S, Storms RK, Veronneau S, Voet M, Volckaert G, Ward TR, Wysocki R, Yen GS, Yu K, Zimmermann K, Philippsen P, Johnston M, Davis RW (1999) Functional characterization of the *S. cerevisiae* genome by gene deletion and parallel analysis. *Science* **285:** 901–906

Yang Y, Fang S, Jensen JP, Weissman AM, Ashwell JD (2000) Ubiquitin protein ligase activity of IAPs and their degradation in proteasomes in response to apoptotic stimuli. *Science* **288:** 874–877

Yao T, Cohen RE (2002) A cryptic protease couples deubiquitination and degradation by the proteasome. *Nature* **419:** 403–407

THE JOURNAL OF BIOLOGICAL CHEMISTRY VOL. 281, NO. 52, pp. 39891–39896, December 29, 2006

Protein Phosphatase 6 Down-regulates TAK1 Kinase Activation in the IL-1 Signaling Pathway*

Received for publication, August 24, 2006, and in revised form, October 30, 2006 Published, JBC Papers in Press, November 1, 2006, DOI 10.1074/jbc.M608155200

Taisuke Kajino[‡], Hong Ren[§], Shun-ichiro Iemura[¶], Tohru Natsume[¶], Bjarki Stefansson[‖], David L. Brautigan[‖], Kunihiro Matsumoto[‡], and Jun Ninomiya-Tsuji[**‡‡1]**

*From the [‡]Department of Molecular Biology, Graduate School of Science, Nagoya University, Nagoya 464-8602, Japan, [§]Cell Signaling Technology, Danvers, Massachusetts 01923, [¶]National Institutes of Advanced Industrial Science and Technology, Biological Information Research Center, Kohtoh-ku, Tokyo 135-0064, Japan, [‖]Center for Cell Signaling, University of Virginia School of Medicine, Charlottesville, Virginia 22908, **Solution-oriented Research for Science and Technology, Japan Science and Technology Agency, Japan, and [‡‡]Department of Environmental and Molecular Toxicology, North Carolina State University, Raleigh, North Carolina 27695-7633*

TAK1 (transforming growth factor β-activated kinase 1) is a serine/threonine kinase that is a mitogen-activated protein kinase kinase kinase and an essential intracellular signaling component in inflammatory signaling pathways. Upon stimulation of cells with inflammatory cytokines, TAK1 binds proteins that stimulate autophosphorylation within its activation loop and is thereby catalytically activated. This activation is transient; it peaks within a couple of minutes and is subsequently down-regulated rapidly to basal levels. The mechanism of down-regulation of TAK1 has not yet been elucidated. In this study, we found that toxin inhibition of type 2A protein phosphatases greatly enhances interleukin 1 (IL-1)-dependent phosphorylation of Thr-187 in the TAK1 activation loop as well as the catalytic activity of TAK1. From proteomic analysis of TAK1-binding proteins, we identified protein phosphatase 6 (PP6), a type-2A phosphatase, and demonstrated that PP6 associated with and inactivated TAK1 by dephosphorylation of Thr-187. Ectopic and endogenous PP6 co-precipitated with TAK1, and expression of PP6 reduced IL-1 activation of TAK1 but did not affect osmotic activation of MLK3, another MAPKKK. Reduction of PP6 expression by small interfering RNA enhances IL-1-induced phosphorylation of Thr-187 in TAK1. Enhancement occurred without change in levels of PP2A showing specificity for PP6. Our results demonstrate that PP6 specifically down-regulates TAK1 through dephosphorylation of Thr-187 in the activation loop, which is likely important for suppressing inflammatory responses via TAK1 signaling pathways.

TAK1[2] (transforming growth factor β-activated kinase 1) is a member of the mitogen-activated protein kinase kinase kinase (MAPKKK) family and is activated not only by transforming growth factor β but also by proinflammatory cytokines including interleukin-1 (IL-1) and tumor necrosis factor (1–3). Genetic studies using TAK1-deficient cells have demonstrated that TAK1 is an indispensable signaling intermediate in tumor necrosis factor and IL-1 signaling pathways (4–6). In the proinflammatory signaling pathways, TAK1 is activated through ligand-dependent assembly of a TAK1 signaling complex containing tumor necrosis factor receptor-associated factor (TRAF) TAK1 binding partners, TAK1-binding proteins 1, 2, and 3 (TAB1, TAB2, and TAB3) (2, 4–13). TAK1, in turn, stimulates two downstream pathways; one is the MAPK cascades to activate c-Jun N-terminal kinase (JNK) and p38 MAPK, and the other is the IκB kinase pathway ultimately leading to NF-κB activation (2, 4, 5, 14).

Many kinases are phosphorylated in the kinase activation loop located between the conserved sequence DFG of kinase subdomain VII and APE of kinase subdomain VIII (15). The activation loop is important for substrate recognition, and phosphorylation in this segment is required to allow correct alignment of the substrates to the catalytic site. In many cases, phosphorylation within the activation loop is mediated by upstream kinases in the kinase cascades (16). However, in some kinases, autophosphorylation occurs in this segment following stimuli-dependent conformational change (17–20). The kinase activation loop of TAK1 contains phosphorylation sites at Thr-184, Thr-187, and Ser-192. Unphosphorylatable amino acid substitutions of any of these residues abolish the catalytic activity of TAK1 (8, 21). Proinflammatory cytokines increase phosphorylation of TAK1 within the activation loop (8, 21). Catalytic activity of TAK1 is required for this phosphorylation, suggesting that TAK1 autophosphorylates its activation loop. Upon cytokine stimulation, TAK1 autophosphorylation is induced presumably through the conformational change due to assembly of the signaling complex, which converts TAK1 into a catalytically active form. Among the phosphorylation sites in the TAK1 activation loop, it has so far been established that phosphorylation at Thr-187 correlates with activation of TAK1 (22).

* This work was supported by special grants for Solution-oriented Research for Science and Technology and Advanced Research on Cancer from the Ministry of Education, Culture, and Science of Japan (to K. M.) and by National Institutes of Health Grants GM068812 and AR050972 (to J. N.-T.), and CA077584 (to D. L. B.). The costs of publication of this article were defrayed in part by the payment of page charges. This article must therefore be hereby marked "*advertisement*" in accordance with 18 U.S.C. Section 1734 solely to indicate this fact.

[1] To whom correspondence should be addressed. Tel.: 919-513-1586; Fax: 919-515-7169; E-mail: Jun_Tsuji@ncsu.edu.

[2] The abbreviations used are: TAK1, transforming growth factor β-activated kinase 1; MAPKKK, mitogen-activated protein kinase kinase kinase; IL-1, interleukin-1; TAB1, TAK1-binding protein 1; JNK, c-Jun N-terminal kinase; PP6, protein phosphatase 6; PP2A, type 2A protein phosphatase; OA, okadaic acid; MLK, mixed lineage protein kinase 3; siRNA, small interfering RNA; TRAF, tumor necrosis factor receptor-associated factor; HA, hemagglutinin.

TAK1 is activated in a transient manner (23). IL-1 activates TAK1 within 1–2 min, and the activation peaks at 3–5 min and declines to the basal levels within 15–30 min after stimulation. Although TAK1 activation has been determined to some extent as described above, the mechanism by which TAK1 is down-regulated remains largely unknown. In general, the level of protein phosphorylation is controlled by the balanced activities of protein kinases and protein phosphatases. Indeed, TAK1 activity is known to be regulated by protein phosphatase PP2C family members in the unstimulated state (24, 25). In this study, we found that inhibition of type 2A protein phosphatases results in hyperphosphorylation and hyperactivation of TAK1 in response to IL-1 stimulation. The protein Ser/Thr phosphatase family comprises the type 1 and type 2A phosphatases, and these are the major protein phosphatases that play an important role in the regulation of cell growth and a diverse set of cellular proteins, including metabolic enzymes, ion channels, hormone receptors, and kinase cascades (26). Protein phosphatase 4 (PP4) and protein phosphatase 6 (PP6) have been identified as novel phosphatases and have been classified as type 2A phosphatase family members based on their sequence homology (27–29). However, relative to PP2A, much less is known about the functions of PP4 and PP6. Recently, PP6 has been implicated in opposing NF-κB activation by control of IκBε degradation (30). We here found that TAK1 associates with PP6 and that PP6 dephosphorylates and inactivates TAK1. We also show that reduction of PP6 expression increases phosphorylation of IL-1-induced TAK1. Our results suggest that PP6 is a negative regulator of TAK1.

EXPERIMENTAL PROCEDURES

Chemicals, Plasmids, and Antibodies—Tautomysin, okadaic acid, cyclosporin A, and calculin A were purchased from Calbiochem. Recombinant human IL-1β was purchased from Roche Applied Science. The mammalian expression vectors for HA-tagged TAK1 (HA-TAK1), FLAG-tagged TAK1 (FLAG-TAK1), and TAB1 have been described previously (2, 10, 23). A catalytically inactive version of PP6, PP6-D84N, was prepared by QuikChange (Stratagene) according to the manufacturer's instruction. Anti-phospho-TAK1 (Thr-187) antibody (Cell Signaling), anti-TAK1 antibody (2), anti-HA monoclonal antibody 16B12 (Covance), anti-FLAG monoclonal antibody M2 (Sigma), anti-mixed lineage protein kinase 3 (MLK3), anti-phospho-MLK3 (Thr-277/Ser-281) (Cell Signaling), anti-PP2A (Santa Cruz), anti-PP6 antibody (Sigma), and anti-β-catenin (BD Biosciences) were used.

Cell Cultures—293 cells, 293 IL-1RI cells, were cultured in Dulbecco's modified Eagle's medium plus 10% bovine growth serum (HyClone) or fetal bovine serum. Transfection of 293 cells was carried out according to the calcium phosphate precipitation method.

siRNAs—siRNAs targeted against human PP6 were purchased from Dharmacon Inc. Two siRNA against the sequences PP6-1 (^{47}GCA AGT ACC TGC CAG AGA A^{65}) and PP6-2 (^{893}GAA CGA CAA CGC CAT ATT T^{911}) were used. A pool of three siRNAs for human PP2A was purchased from B-Bridge, (target sequences ^{333}CAC CAT TCT TCG AGG GAA T^{351}, ^{663}GCA AGA TAT TTC TGA GAC A^{681}, and 3′ untranslated region GGA AAT GGG AAG AGC AAC A). Control siRNA against unrelated nucleotide sequence was purchased from Ambion (*Silencer* negative Control 1 siRNA). The siRNA duplexes were transfected into 293 IL-1R cells using Oligofectamine reagent (Invitrogen). Cells were incubated in 30% fetal bovine serum for 48 h post-transfection and then stimulated with IL-1.

Immunoprecipitation and Immunoblotting—Whole cell extracts were prepared in lysis buffer (20 mM HEPES, pH 7.4, 150 mM NaCl, 12.5 mM β-glycerophosphate, 1.5 mM $MgCl_2$, 2 mM EGTA, 10 mM NaF, 2 mM dithiothreitol, 1 mM Na_3VO_4, 1 mM phenylmethylsulfonyl fluoride, 20 μM aprotinin, 0.5% Triton X-100). Proteins from these cell lysates were immunoprecipitated with 1 μg of various antibodies and 15 μl of protein G-Sepharose (GE Healthcare). The immune complexes were washed three times with wash buffer containing 20 mM HEPES, pH 7.4, 500 mM NaCl, and 10 mM $MgCl_2$ and once with rinse buffer containing 20 mM HEPES, pH 7.4, 150 mM NaCl, and 10 mM $MgCl_2$ and suspended in 30 μl of rinse buffer. For immunoblotting, the immunoprecipitates or cell lysates were resolved on SDS-PAGE and transferred to Hybond-P membranes (GE Healthcare). The membranes were immunoblotted with various antibodies, and bound antibodies were visualized with horseradish peroxidase-conjugated antibodies against rabbit or mouse IgG using the ECL Western blotting system (GE Healthcare) or SuperSignal West Femto sensitivity substrate (Pierce).

In Vitro Kinase Assay—Immunoprecipitates were incubated with 1 μg of bacterially expressed MKK6 in 10 μl of kinase buffer containing 10 mM HEPES, pH 7.4, 1 mM dithiothreitol, 5 mM $MgCl_2$, and 5 μCi of [γ-^{32}P]ATP (3,000 Ci/mmol) at 25 °C for 2 min. Samples were fractionated by 10% SDS-PAGE and visualized by autoradiography.

In Vitro Dephosphorylation Assay—Purified PP2A was purchased from Millipore/Upstate. HA-TAK1 was activated by co-expression of TAB1 in 293 cells and was immunoprecipitated with anti-HA, incubated with the purified PP2A for 30 min at 30 °C.

RESULTS

Inhibition of Type 2A Phosphatase Activity Increases IL-1-induced Phosphorylation of TAK1—TAK1 is activated through its autophosphorylation within the activation loop induced by binding of proteins such as TAB1, TAB2, and TRAFs and is rapidly down-regulated (8, 22, 23). The mechanism by which TAK1 is down-regulated has not yet been elucidated, but it is likely to involve protein phosphatases. Indeed, both TAK1 phosphorylation and activation are regulated by PP2C family (also known as MPP) phosphatases, which participate in silencing TAK1 basal activity in the unstimulated state (24, 25). To further address which protein phosphatases reverse stimuli-induced TAK1 activation, we examined the effects of protein phosphatase inhibitors on IL-1-induced TAK1 phosphorylation. The 293 IL-1RI cell line, which stably expresses IL-1 receptor, was stimulated by IL-1 in the presence or absence of different phosphatase inhibitors: 1) tautomycin, an inhibitor of PP1; 2) okadaic acid (OA), an inhibitor of the PP2A family; 3) cyclosporin A, an inhibitor of PP2B; or 4) calyculin A, an inhib-

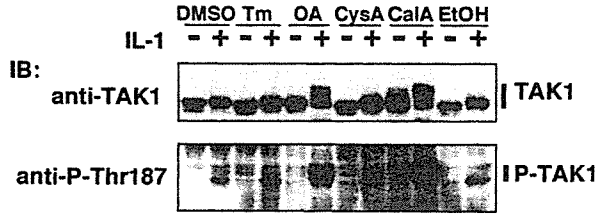

FIGURE 1. **Effect of protein phosphatase inhibitors on TAK1 phosphorylation.** Cultures of 293 IL-1RI cells were treated with 1 μM tautomycin (*Tm*), 100 nM okadaic acid (*OA*), or 1 μM cyclosporin A (*CysA*) for 6 h or 20 nM calyculin A (*CalA*) for 40 min or the vehicle Me_2SO (*DMSO*) or ethanol (*EtOH*) for 6 h followed by treatment with IL-1 (5 ng/ml) for 5 min. Cell lysates were subjected to immunoblotting (*IB*) with anti-TAK1 and anti-P-Thr-187.

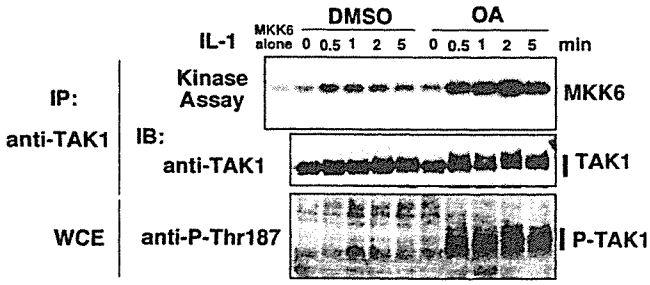

FIGURE 2. **Effect of OA on IL-1-induced activation of TAK1.** 293 IL-RI cells were pretreated with 100 nM okadaic acid or vehicle Me_2SO (*DMSO*) for 5 h followed by addition of IL-1 (5 ng/ml). Proteins from the cell lysates were immunoprecipitated with anti-TAK1 and subjected to *in vitro* kinase assay using MKK6 as an exogenous substrate (*top panel*) and immunoblotting with anti-TAK1 (*middle panel*). The phosphorylated TAK1 was detected with anti-P-Thr-187 (*bottom panel*). *IP*, immunoprecipitation; *IB*, immunoblotting; *WCE*, whole cell extracts.

itor of both the PP1 and the PP2A families (Fig. 1). Although OA can inhibit both PP1 and PP2A at high concentrations, OA at the concentration of 100 nM was used for relatively selective inhibition of the PP2A family (31). Upon IL-1 treatment TAK1 was autophosphorylated and it migrated more slowly than unstimulated TAK1 on SDS-PAGE (Fig. 1, *upper panel*) as described previously (8). Phosphorylation of TAK1 in the activation loop was monitored by immunoblotting with a phospho-specific antibody that recognized phosphorylated TAK1 at Thr-187 (anti-P-Thr-187) (Fig. 1, *lower panel*). IL-1-induced phosphorylation at Thr-187 was barely detected without phosphatase inhibitor, but either OA or calyculin A greatly enhanced the IL-1-dependent phosphorylation at Thr-187 and showed a large mobility shift of TAK1 on SDS-PAGE. In contrast, neither tautomycin nor cyclosporine A enhanced the TAK1 phosphorylation at Thr-187 or altered mobility in SDS-PAGE. These results suggest that inhibition of the PP2A family enhances the phosphorylation of TAK1 at Thr-187. To assess the role of PP2A family members on TAK1, we used 100 nM OA for the subsequent experiments.

Inhibition of the PP2A Family Increases IL-1-induced Activation of TAK1—We examined the kinetics of TAK1 activation in the absence and presence of OA (Fig. 2). Catalytic activity of TAK1 was measured using MKK6 as a specific substrate. IL-1 addition to cells stimulated TAK1 activity at 0.5 and 1.0 min, and the activity declined rapidly thereafter, returning to basal by 5 min. Addition of OA significantly enhanced IL-1-dependent activation of TAK1. The peak levels of TAK1 catalytic activity were greatly increased, and the activity peaked at 2 min and

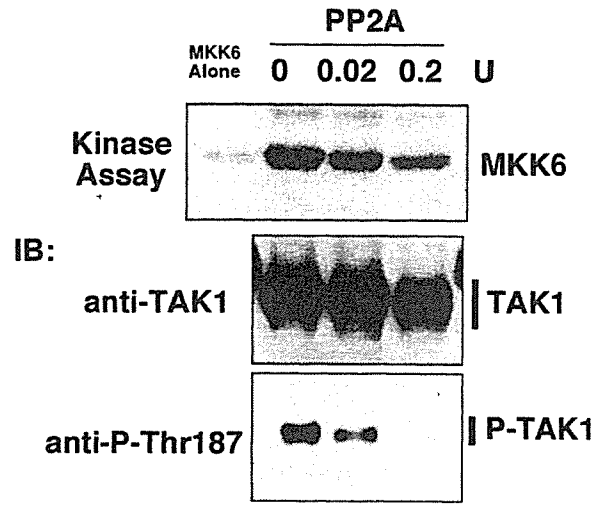

FIGURE 3. **PP2A dephosphorylates and inactivates TAK1.** HA-TAK1 and TAB1 were co-expressed in 293 cells and precipitated with anti-HA. The immunoprecipitate first was incubated with 0.02 or 0.2 units of purified PP2A (dimer of AC subunits) and subjected to *in vitro* kinase assay using MKK6 as an exogenous substrate (*top panel*). Total TAK1 was detected with anti-TAK1 (*middle panel*), and phosphorylated TAK1 was detected with anti-P-Thr-187 (*bottom panel*). *IB*, immunoblotting.

was sustained longer (>5 min) compared with that in OA-untreated cells. The phosphorylation of TAK1 at Thr-187 enhanced by OA was correlated with the kinetics of OA-induced TAK1 activation. These data demonstrate that inhibition of PP2A family phosphatases by OA enhances IL-1-dependent phosphorylation and activation of TAK1.

PP2A Can Dephosphorylate and Inactivate TAK1 in Vitro—Upon cell stimulation, TAK1 binds to the TRAF6-containing complex and autophosphorylates Thr-187 in the activation loop, thereby activating its catalytic activity (8). Therefore, we speculate that a PP2A family phosphatase may down-regulate TAK1 by dephosphorylating Thr-187 in the TAK1 activation loop. We examined whether PP2A could directly dephosphorylate Thr-187 and inactivate TAK1. We isolated an active form of TAK1 from cells co-expressing TAK1 together with its activator subunit TAB1. Ectopically expressed TAB1 induces autophosphorylation of TAK1 at the activation loop, as does treatment of cells with IL-1 (8). The activated TAK1 was immunoprecipitated and incubated with purified PP2A (Fig. 3). PP2A dephosphorylated Thr-187 in the TAK1 activation loop and inactivated TAK1. Collectively, these results suggest that a PP2A family phosphatase negatively regulates TAK1 by dephosphorylating Thr-187 in the activation loop of TAK1.

PP6 Interacts with TAK1—To identify the TAK1 endogenous phosphatase, we immunoprecipitated FLAG-tagged TAK1 from transiently transfected cells. The immunocomplex was digested, and the peptides were analyzed by using a nano-scale liquid chromatography system with collision-induced dissociation tandem mass spectrometry (32). Several peptides were found to correspond to TAB1. One peptide yielded the sequence YGNANAWRYCTK, and it corresponded to protein phosphatase 6 (PP6) catalytic subunit. To confirm the interaction of TAK1 with PP6, we conducted the immunoprecipitation assay (Fig. 4*A*). FLAG-TAK1 and HA-tagged PP6 catalytic subunit (HA-PP6) were co-expressed in 293 cells. FLAG-TAK1

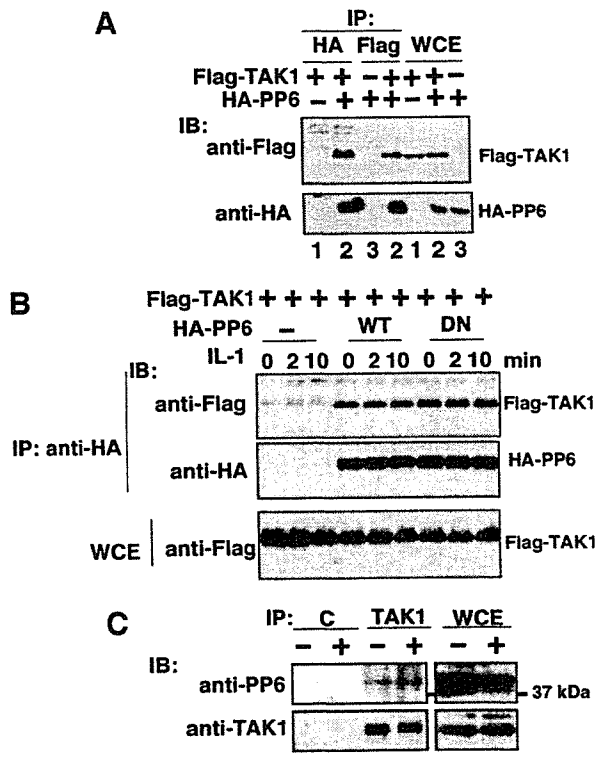

FIGURE 4. **Association of TAK1 with PP6.** *A*, 293 cells were transfected with expression vectors for FLAG-TAK1 and HA-PP6. Proteins from the cell lysates were immunoprecipitated with anti-HA or with anti-FLAG and immunoblotted with anti-FLAG and anti-HA. *IP*, immunoprecipitation; *IB*, immunoblotting; *WCE*, whole cell extracts. *B*, 293 IL-1RI cells were transfected with expression vectors for FLAG-TAK1, HA-PP6 wild type (*WT*), or a catalytically inactive version of HA-PP6 D84N (*DN*). At 36 h post-transfection, cells were treated with 5 ng/ml IL-1. Proteins from the cell lysates were immunoprecipitated with anti-HA and immunoblotted with anti-FLAG and anti-HA. *IP*, immunoprecipitation; *IB*, immunoblotting; *WCE*, whole cell extracts. *C*, 293 IL-1RI cells were treated with or without 5 ng/ml IL-1 for 1 min. Endogenous proteins were immunoprecipitated with anti-TAK1 (*TAK1*) or with control IgG (*C*), and co-precipitated PP6 was detected with anti-PP6. *IP*, immunoprecipitation; *IB*, immunoblotting; *WCE*, whole cell extracts.

co-precipitated with HA-PP6, and the interaction was confirmed by the reciprocal anti-HA immunoprecipitation. We asked whether stimulation of TAK1 and the catalytic activity of PP6 affect the interaction. We co-expressed FLAG-TAK1 with HA-PP6 wild type and a catalytically inactive form of PP6 (PP6-D84N) in 293 IL-1RI cells and treated cells with IL-1 (Fig. 4*B*). TAK1 associated with PP6 independent of catalytic activity of PP6. The interaction was not altered by IL-1 stimulation. These results suggest that PP6 is a constitutive binding partner of TAK1 with or without IL-1 stimulation.

To verify the physiological TAK1-PP6 interaction, we examined whether endogenous TAK1 associated with PP6. Cell extracts from cells treated with or without IL-1 were prepared and endogenous TAK1 was immunoprecipitated (Fig. 4*C*). PP6 was co-precipitated with TAK1 with and without IL-1 stimulation of cells. This indicated that endogenous PP6 interacts with TAK1.

PP6 Dephosphorylates and Inactivates TAK1—We examined whether PP6 can dephosphorylate TAK1. PP6 wild type or catalytically inactive form of PP6 was overexpressed in 293 IL-1RI cells, and cells were stimulated with IL-1. The phosphorylation

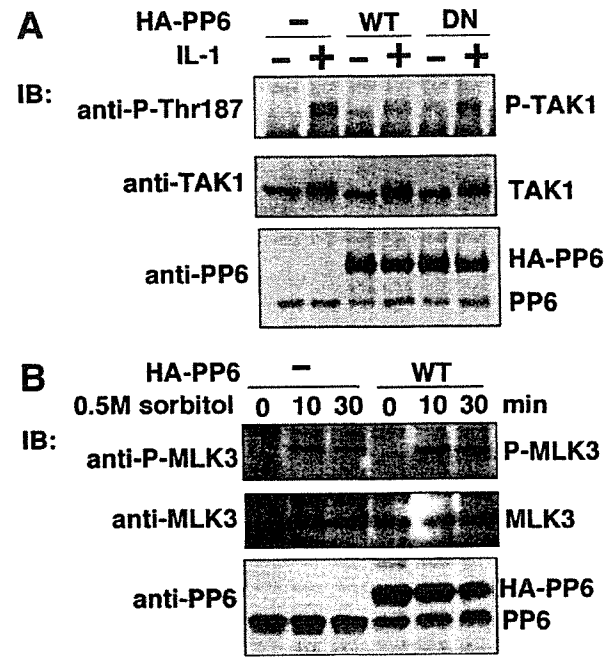

FIGURE 5. **Phosphorylation of TAK1 depends on PP6.** *A*, 293 IL-1RI cells were transfected with an empty vector (−) or with expression vectors for HA-PP6 wild type (*WT*) and a catalytically inactive version of HA-PP6 D84N (*DN*). At 48 h post-transfection, cells were treated with 5 ng/ml IL-1 for 1 min. Cell lysates were subjected to immunoblotting with anti-P-Thr-187, anti-TAK1, and anti-PP6. *IB*, immunoblotting. *B*, 293 cells were transfected with an empty vector (−) or with expression vector for HA-PP6 wild type (*WT*). At 48 h post-transfection, cells were treated with 0.5 M sorbitol for 10 or 30 min. Cell lysates were subjected to immunoblotting with anti-phospho-MLK3, anti-MLK3, and anti-PP6. *IB*, immunoblotting.

of TAK1 was monitored by anti-P-Thr-187 antibody (Fig. 5*A*). We found that increased expression of PP6 reduced IL-1-dependent phosphorylation at Thr-187 of TAK1. To determine whether PP6 action is specific to TAK1 among the family members of MAPKKKs, we examined the effect of PP6 overexpression on osmotic stress-induced MLK3 activation. MLK3 is phosphorylated and activated upon osmotic stress. 293 cells were treated with 0.5 M sorbitol, and the phosphorylated form of MLK3 was detected with a phospho-specific MLK3 antibody (Fig. 5*B*). Ectopic expression of PP6 did not alter the phosphorylation status of MLK3.

We examined whether PP6 levels affected regulation of TAK1. We tested down-regulation of PP6 by siRNA in IL-1-induced activation of TAK1. Different siRNAs (PP6-1 and PP6-2) targeted against two sequences in human PP6 were used. The synthetic siRNA duplexes were transfected into 293 IL-1RI cells, and the reduction of PP6 expression was monitored by immunoblotting of PP6 (Fig. 6*A*). Both siRNAs resulted in a 60–80% decrease in the level of PP6 protein. Specificity of these siRNAs was confirmed by showing no change in the protein levels of PP2A and the unrelated protein β-catenin. Knock down of PP6 led to an increased phosphorylation of Thr-187 TAK1 in IL-1-stimulated cells (Fig. 6*B*). In contrast, siRNAs targeted against PP2A did not alter the phosphorylation of Thr-187 of TAK1 (Fig. 6*C*). These results confirm that PP6 is the negative regulator of TAK1 activation by IL-1 stimulation.